IMAGE-BASED NON-CONTACT CONDUCTIVITY PREDICTION FOR INKJET PRINTED ELECTRODES AND FOLLOW-UP WORK OF TONER USAGE PREDICTION FOR LASER ELECTRO-PHOTOGRAPHIC PRINTERS

A Thesis

Submitted to the Faculty

of

Purdue University

by

Yang Yan

In Partial Fulfillment of the

Requirements for the Degree

of

Master of Science in Electrical and Computer Engineering

August 2019

Purdue University

West Lafayette, Indiana

THE PURDUE UNIVERSITY GRADUATE SCHOOL
STATEMENT OF THESIS APPROVAL

Dr. Jan P. Allebach, Chair

School of Electrical and Computer Engineering

Dr. George T. C. Chiu

School of Mechanical Engineering

Dr. Amy R. Reibman

School of Electrical and Computer Engineering

Approved by:

Dr. Dimitrios Peroulis

Head of the School Graduate Program

ACKNOWLEDGMENTS

I would like to thank my advisor Professor Jan P. Allebach for providing me the opportunity to work with him. Without his advice and expertise, all these researches would not have happened. I also would like to express my special thanks to Professor Chiu for granting me the access to instruments in his lab and Professor Shakouri for his active involvement and generous support, without whom the project is non-existence. I want to express my gratitude to my committee members including Professor Reibman and Professor Chiu. Their feedback and advice is significant for thesis writing process.

I would like to thank the research sponsor for the toner usage prediction project, the Hewlett-Packard Company, which gives us generous support. Referring to the toner usage prediction project, I also would like to thank to my supervisor Terry Nelson. I really enjoy the time working with him.

I sincerely appreciate all EISL members and SMART members, especially Mengqi Gao, Tongyang Liu, Qingyu Yang, Kerry Maize, Nicholas J. Glassmaker, Guy J. Telesnicki, Muhammed R. Oduncu, Jie Wang, Professor Alexander Wei, and Professor Mukerrem Cakmak, who have either worked with me or provided help and advice during the past two and half years.

I would be remiss to not mention and thank my parents Yuxia Yan and Hongjuan Shen for understanding me to achieve my acedemic goals. I would like to thank all my friends who always give me mental support and love.

TABLE OF CONTENTS

Page

LIST OF TABLES

LIST OF FIGURES

Figure Page

Figure Page

ABBREVIATIONS

BBM	black box model
C	cyan
CMOS	complementary metal-oxide-semiconductor
dpi	dot per inch
EISL	electronic imaging systems laboratory
EP	edge proportion
ER	edge roughness
GP	Gaussian pyramid
GUI	graphical user interface
K	black
LBP	local binary pattern
LSQR	least square
LUT	look up table
M	magenta
MSE	mean square error
R2R	roll-to-roll
RMSE	root mean square error
SMART films	scalable manufacturing of aware and responsive thin films
pL	picoliter(s), equals 10^{-12} liter
Y	yellow

NOMENCLATURE

Ammonium Carbamate	inorganic compound with the formula $NH_4[H_2NCO_2]$

ABSTRACT

Yan, Yang M.S.E.C.E., Purdue University, August 2019. Image-Based Non-Contact Conductivity prediction for Inkjet Printed Electrodes and follow-up work of toner usage prediction for laser electro-photographic printers . Major Professor: Jan P. Allebach.

This thesis includes two parts. The main part is on the topic of conductivity prediction for Inkjet printed silver electrodes. The second part is about the follow-up work of toner usage prediction of laser electro-photographic printers.

Conductivity Prediction For Inkjet Printed Silver Electrodes Recently, electronic devices made with Inkjet printing technique and flexible thin films have attracted great attention due to their potential applications in sensor manufacturing. This imaging system has become a great tool to monitor the quality of Inkjet printed electrodes due to the fact that most thickness or resistance measuring devices can destroy the surface of a printed electrode or even whole electrode. Thus, a non-contact image-based approach to estimate sheet resistance of Inkjet printed electrodes is developed.

The approach has two stages. Firstly, strip-shaped electrodes are systematically printed with various printing parameters. The sheet resistance measurement data as well as images of the electrodes are acquired. Then, based on the real experimental data, the fitting model is constructed and further used in predicting the sheet resistance of the Inkjet printed silver electrodes.

Toner Usage Prediction With the widespread use of laser electro-photographic printers in both industry and households fields, estimation of toner usage has great significance to ensuring the full utilization of each cartridge. The follow-up work is focused on testing and improving feasibility, reliability, and adaptability of the Black

Box Model (BBM) based two-stage strategy in estimating the toner usage. Comparing with previous methods, the training process for the first stage requires less time and disk storage, all while maintaining high accuracy. For the second stage, experiments are performed on various models of printers, with cyan(C), magenta(M), yellow(Y), and black(K) color cartridges.

1. INTRODUCTION

1.1 Motivation

The original design of these printed electrodes were for the manufacturing of Nitrate sensors. In order to construct Nitrate sensors, a transparent ion select membrane PET layer will be coated on top of the silver electrodes. The smoothness of the surface of the electrodes will affect the thickness and unity of the topper coating layer. In this case, keeping the surface of the electrodes intact is essential for future convenience. Though sheet resistance is a quantified parameter that can be used to evaluate the quality of printed silver electrodes, sheet resistance measurement processes always leaves indentations of the measuring probes on the surface of the electrodes as shown in Fig. 2.13. once the measurement is taken. This is not desirable in sensor manufacturing. Thus, with the clear advantage of neither contacting nor destroying to the surface, image capture comes into play.

Due to the characteristic of Inkjet printing techniques, part of the printheads can be clogged while printing. This can happen anytime during the whole printing process which may or may not affect the printing results. Based upon different printing drop spaces and printing drop sizes for each printing job, it is ambiguous and inefficient to justify whether printheads have clogged and whether clogging has ruined the electrodes by only viewing the images of the printed electrodes.

So the image-based and experiment-based prediction of sheet resistance for printed silver electrodes is brought up.

1.2 Related Work

Nowadays, there has been a trend with printing electrodes on flexible thin films for manufacturing flexible and wearable electronic devices, such as Inkjet-printed microelectromechanical transistors [1], metal-polymer-silicon capacitors [2], and Inkjet-printed complementary polymer ring oscillators [3]. Compared to the manufacturing of new devices, less researches are focused on printing quality assessment of Inkjet printed electrodes. One research found in particular refers to the thermal conductivity during laser sintering processes [4], however, no further research have been found that selects sheet resistance as an assessment parameter.

1.3 The Proposed Solution

As shown in the Fig. 1.1, the proposed method for predicting the sheet resistance of Inkjet printed silver electrodes is based on experimental sheet resistance measurement physically on the electrodes and the features extracted from digital images captured on the area where the measurement is taken. In the model fitting process, the prediction model is trained with the features extracted from the digital images as inputs and measured sheet resistance as outputs. Finally, the estimated sheet resistance of the printed silver electrodes can be predicted by using just the images of the electrodes. With that being said, this image-based and experiment-based method is highly reliant on the systematic printing manner and consistency of Inkjet printer operation.

Chapter 2.1 contains details about all the experimental processes including printing, sheet resistance measurement, and image capture. Chapter 2.2 contains the methods of data analysis involving image processing tools when extracting features from the captured digital images and machine learning techniques referring to model training and testing.

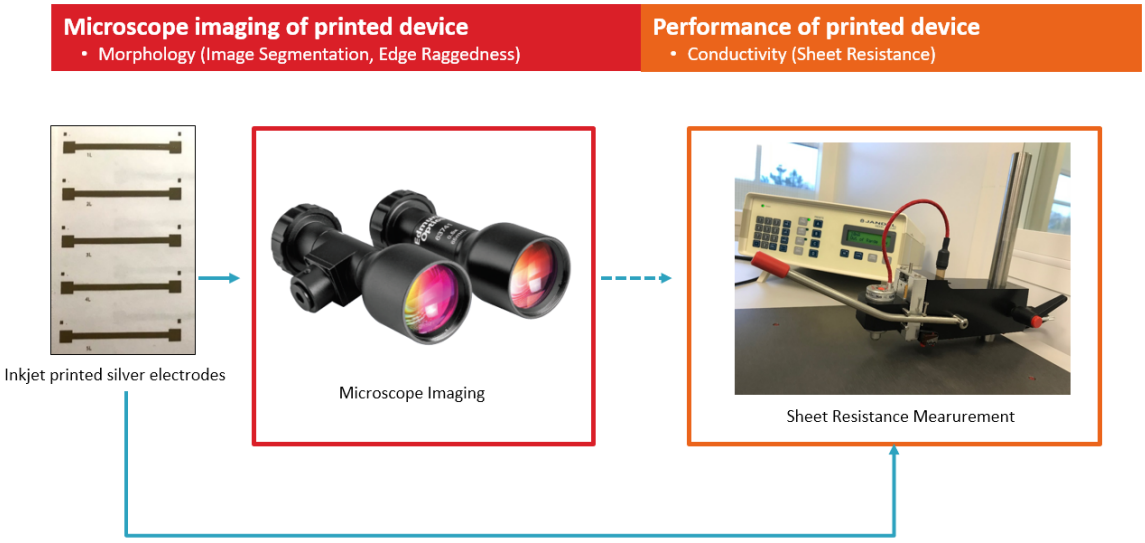

Fig. 1.1. Overview of the Image-Based Experiment-Based Method

2. IMAGE-BASED AND EXPERIMENT-BASED CONDUCTIVITY PREDICTING METHOD FOR INKJET PRINTED SILVER ELECTRODES

The silver electrodes are printed using silver nano-particle ink with different percentage of Ammonium Carbamate loading. The loading percentage is ranging from 3% to 7% to control the viscosity of the ink [5]. This chapter is mainly demonstrating the training and testing process for the electrodes printed with 3% loading of Ammonium Carbamate.

2.1 Experiments and Data Collection Stage

The silver electrodes are systematically printed with different ink drop size cartridges (1 pL/10 pL) and drop spacing with the same silver nano-particle ink with 3% Ammonium Carbamate loading using FUJI Film Dimatix Inkjet printer. To collect data, sheet resistance of all the electrodes is measured with Jandel multi-height probes in clean room. On the same area where the sheet resistance measurement is taken, digital images are captured with a 0.5x magnification telecentric lens and a progressive scan CMOS camera.

2.1.1 Inkjet Printing with Fuji Film Dimatix

Printing Device

Referring to the introduction from FUJI Film, the Dimatix Materials Printer [6] (abbreviated as Dimatix) is a cost-effective, easy-to-use precision materials deposition system designed for research and development as well as feasible testing. As shown in Fig. 2.1, Dimatix has x,y,and z stage and heated vacuum platen. It is manufactured

with built-in drop jetting observation system (also called drop watcher in its PC controllable GUI software, as shown in the Fig. 2.2) and fiducial camera for substrate alignment and measurement. The most convenient feature of Dimatix is its disposable supplement package (Fig. 2.3). It includes fluid module containing a cartridge and an ink injection needle, jetting module with printheads of 1 pL or 10 pL drop size, and a cleaning pad. In this case, every print job starts with a brand new printhead set, which prevent polution in ink and clogging issue from very beginning.

The detailed printing procedure is in appendix A.

Fig. 2.1. Dimatix Materials Printer [6]

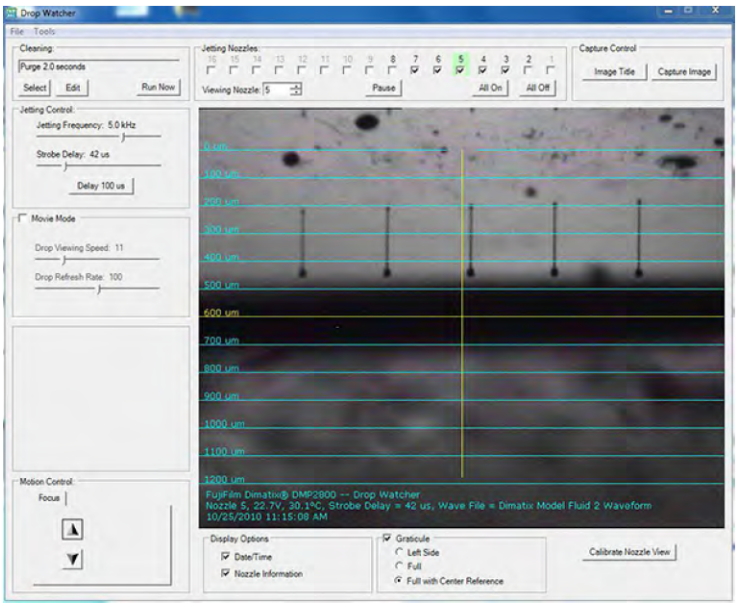

Fig. 2.2. Dimatix Built-In Tool: Drop Watcher

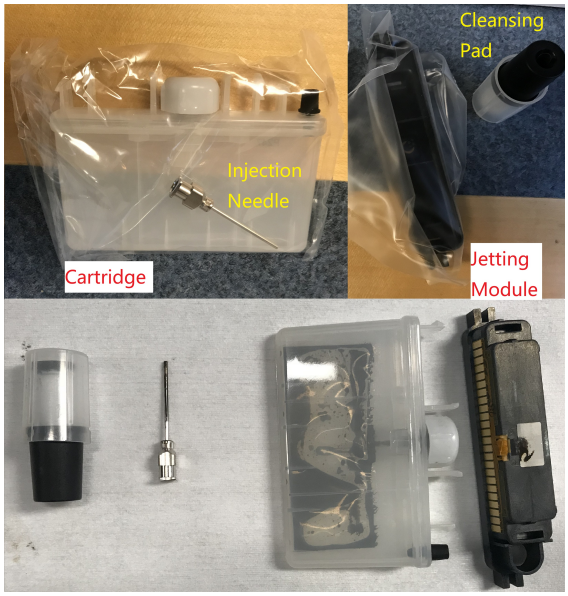

Fig. 2.3. Dimatix Disposable Supplement Package. Top Row: New Condition; Bottom Row: Used Condition

Ink and Printing Substrate

Before printing the electrodes, several items need to be prepared. Silver ink needs to be mixed with Ammonium Carbamate salt in sonication bath (Fig. 2.4). This is a patented technique published in 2012 [5]. Adding any portion of Ammonium Cabamate prevents the oxidation of the silver ink resulting in better conductivity for printed products and stable nature. The substrate used in printing is called Novele (Fig. 2.5), which is a transparent flexible thin film and designed for conductive Inkjet inks.

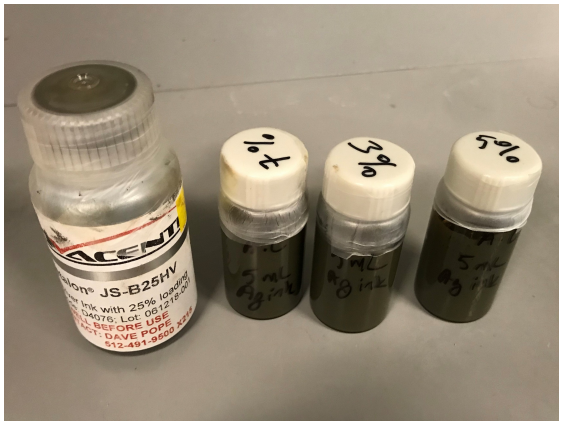

Fig. 2.4. Silver Nano-Particle Ink Mixed with 3%, 5%, and 7% Loading of Ammonium Carbamate

Fig. 2.5. The Transparent Thin Film Substrate: Novele

Table 2.1.
Printing Plan

Print Drop Size (10 pL/1 pL)	**Print Drop Space (μm)**
10 pL	40 (635 dpi)
	25 (1016 dpi)
	20 (1270 dpi)
1 pL	25 (1016 dpi)
	20 (1270 dpi)
	10 (2540 dpi)

Printing Plan

The printing plan is shown in the Table 2.1. At least 20 of the electrodes are printed on one sheet with parameters specified in each row. Dimensions of one electrode as well as a whole sheet of printed electrodes is shown in the Fig. 2.6 and Fig. 2.7 on next page. Time consumed for printing one sheet of electrodes usually ranges from 1 hour to 10 hours according to its print drop spacing. The smaller the print drop spacing is, the more time is required. When print drop spacing is too small, the surface of the printed electrode does not dry in room temperature for over 20 hours since too much ink is deposited. So those are excluded from the table. After printing, each printed sheet is stored in plastic zip-lock bags for preserving a dry and intact condition for storage and transportation purposes.

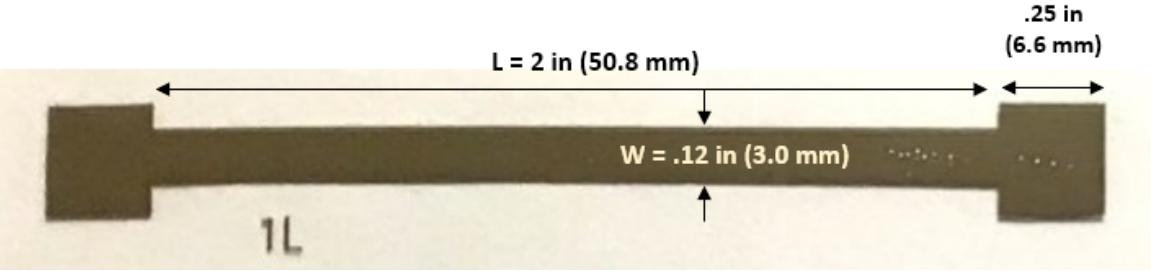

Fig. 2.6. Dimensions of the Electrodes

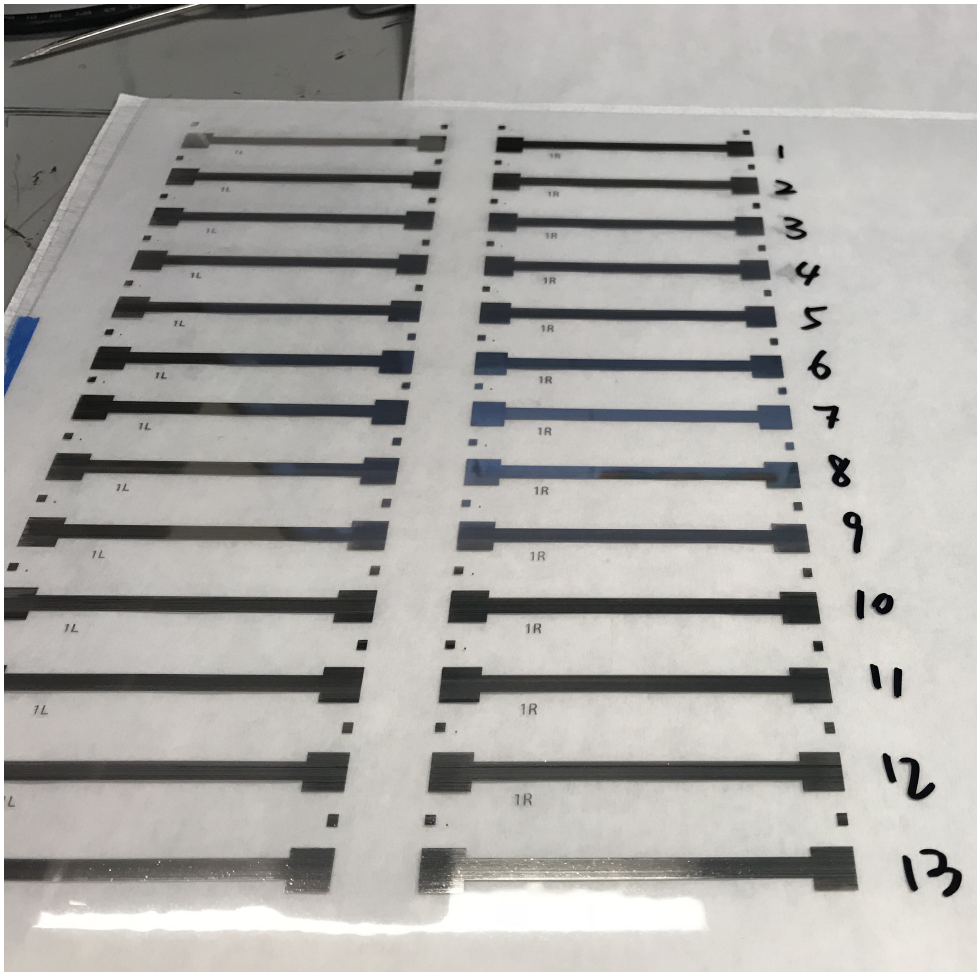

Fig. 2.7. Sample of Printed Electrodes For One Set of Parameter

2.1.2 Data Collection

Sheet Resistance Measurements

After electrodes are printed, sheet resistance measurement is taken on five positions for each electrodes using Jandel multi-height probe as shown in Fig. 2.8. The device is designed to perform multiple electrical measurements for samples with varying thickness. Thus, before performing the measurement, the height of the probes need to be adjusted according to the thickness of the target object. And then, the lowest height of the probes where the actual measurement happens is fixed. Every sheet resistance measurement takes about 50 seconds to 5 minutes to settle down referring to every samples.

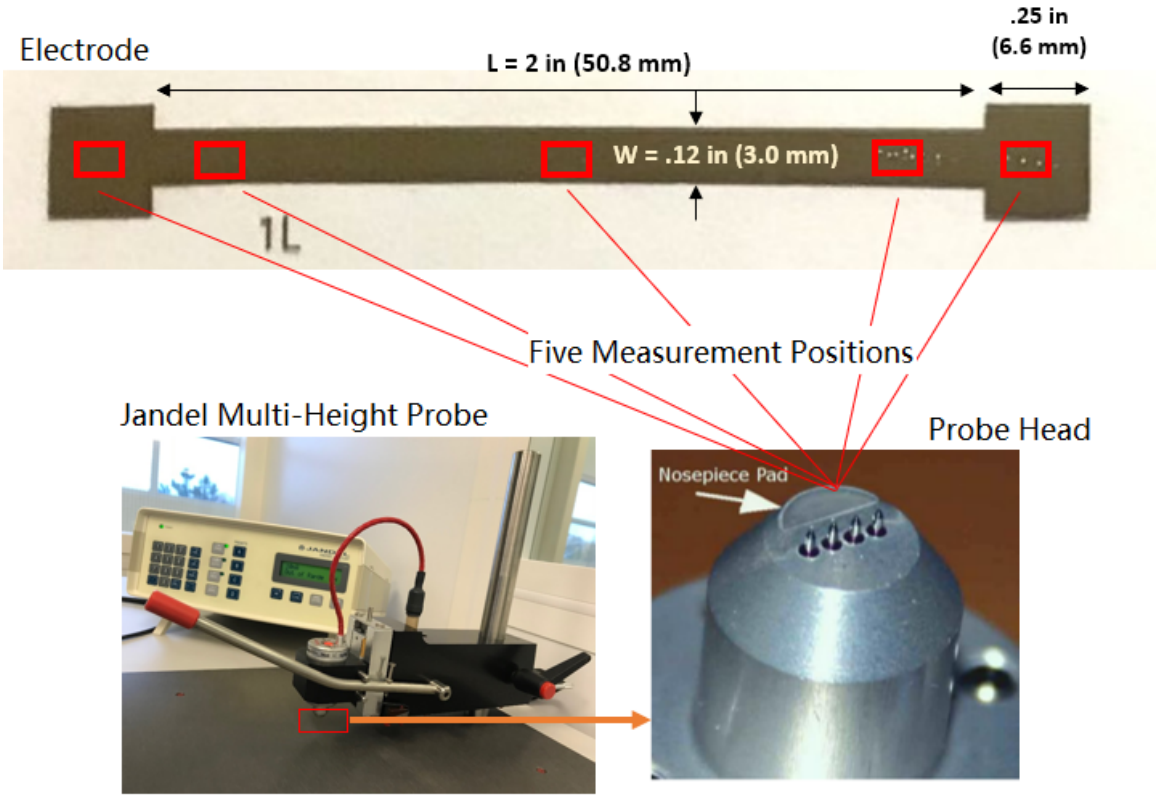

Fig. 2.8. Sheet Resistance Measurement Positions

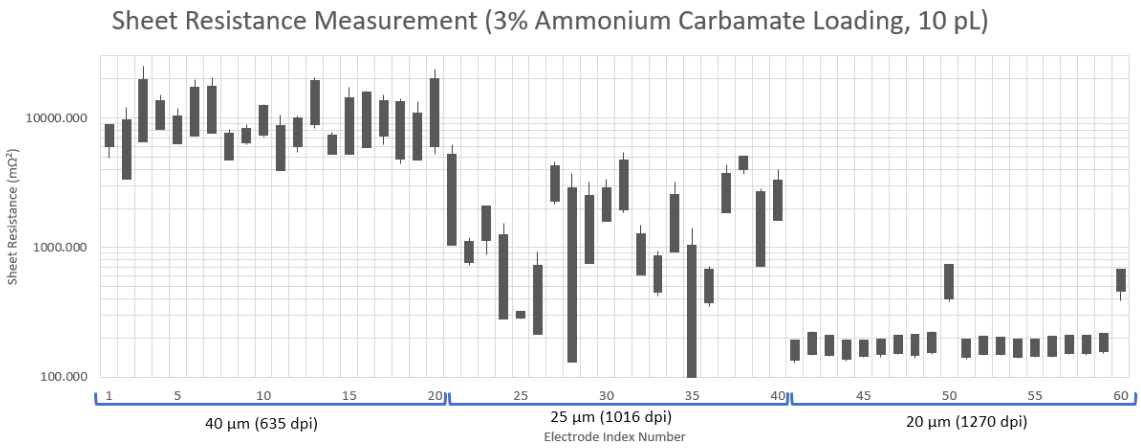

Fig. 2.9. Sheet Resistance Measurement Results for Silver Nanoparticle Ink with 3% Ammonium Carbamate Loading and 10 pL Print Drop Size

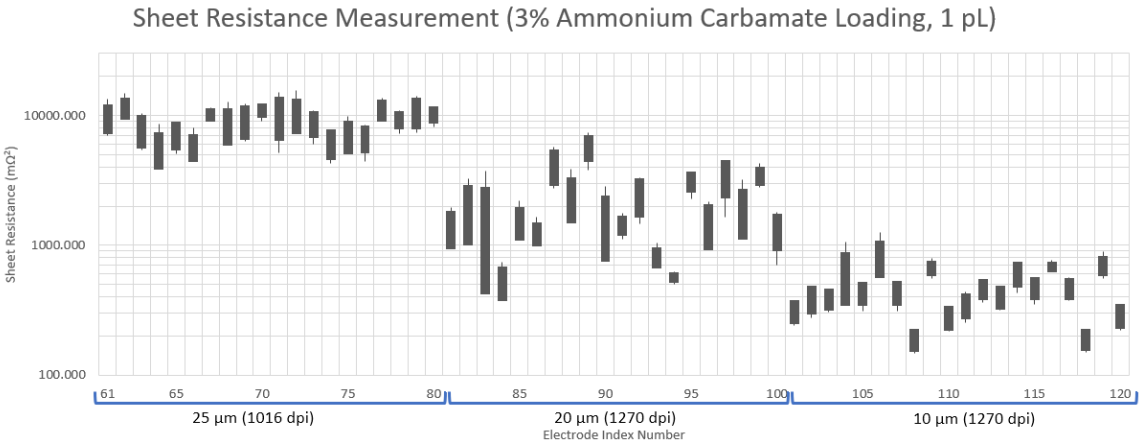

Fig. 2.10. Sheet Resistance Measurement Results for Silver Nanoparticle Ink with 3% Ammonium Carbamate Loading and 1 pL Print Drop Sizes

The sheet resistance measurement results of all the 120 electrodes are shown in Fig. 2.9 and Fig. 2.10. The boxes are the average value plus or minus the standard deviation of the five sheet resistance measurements for one electrode, while the

whiskers are the maximum and minimum measurement values among the five sheet resistances. The sheet resistance values are ploted on log scale for showing the results in different ranges of scales clearly.

Image Capture

Then images are captured on the area where the sheet resistance measurement is taken. Due to the transparency of the substrate, a piece of silicon wafer is put beneath of the imaging area to remove the noise generated by the surface of imaging system operating platform (Fig. 2.11). A 0.5 times magnification telecentric lens(shown in the Fig. 2.12) manufactured by Edmund is used for reducing the color or size changing influenced by the object's relative distance or position in the field of view. All the images are captured right on top of the targeting area with same in-line light source, same light intensity, same aperture and same exposure time. No color correction, filtering, or any other image processing techniques are applied to the captured images. A sample of the captured image is shown in the Fig. 2.13.

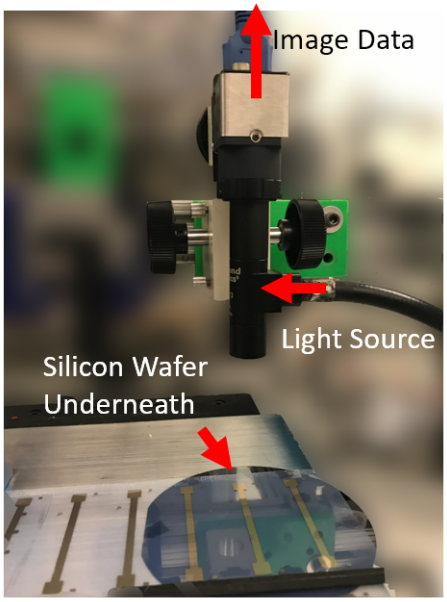

Fig. 2.11. Imaging System

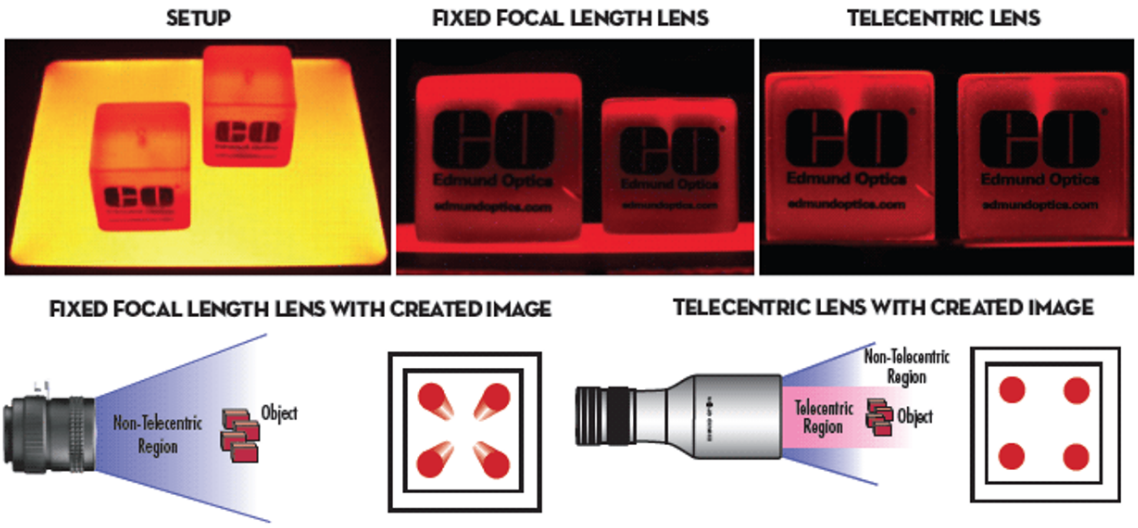

Fig. 2.12. Properties for Telecentric Lens

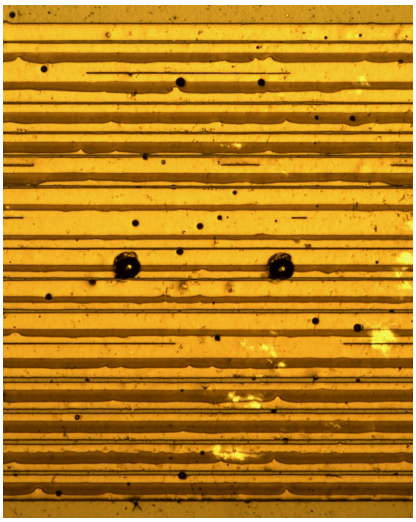

Fig. 2.13. A Image of the Electrode Printed with 10 pL, 25 μm drop size (1016 dpi)

2.2 Data Analysis Stage

2.2.1 Image Features Extraction

It is obvious that the light intensity over the image is not evenly distributed, though the in-line light source socket is fixed on the lens. Therefore, before any image analysis techniques are applied to the images, flat field correction [7] is applied to all of the images. The dark field image (D in Equation 2.1) is taken when the lens is covered and the resulting image of the camera used here is completely dark with 0 values across the whole image. Several flat field images (F in Equation 2.1) are captured when the settings of the light and camera are the same as those when images (R in Equation 2.1) to be corrected are captured. The comparison between the raw image and the corrected image is shown in Fig. 2.14.

$$
\begin{aligned}
C &= (R - D) \times \frac{m}{F - D} \\
&= R \times \frac{m}{F} \\
m &= \frac{\sum_{i=1}^{m} \sum_{j=1}^{n} F(i,j)}{m \times n} \\
where \quad & m = image\,width,\ n = image\,length,\ (i,j) = Pixel\ Position \\
& C = corrected\,image,\ R = raw\,image,\ D = dark\ field\,image \\
& F = average\,image\,of\ all\ flat\ field\,images
\end{aligned}
\tag{2.1}
$$

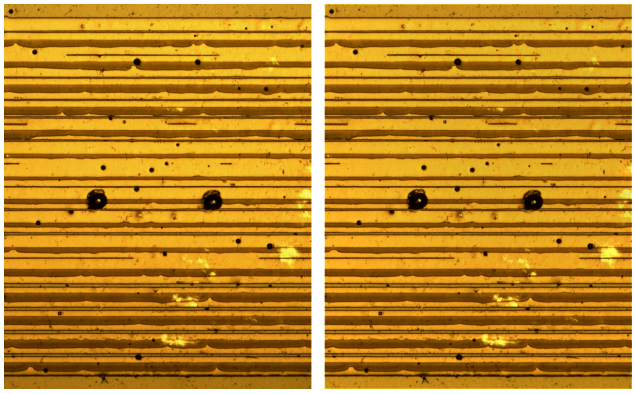

Fig. 2.14. Before (Left) and After (Right) Flat Field Correction Applied to the Image of the Electrode Printed with 10 pL, 25 μm drop size (1016 dpi)

Image Segmentation According To Ink Layers

The two dark circles on the image are the dents left by the middle two probe head of the Jandel probe when doing the sheet resistance measurement. Other than that, the variations in intensity of the colors is caused by various number of print passes, based on analysis on the height measurement report of the printed electrodes from zeta 3-D optical profiler. Strips with darker color are areas that were covered with doubled layers of ink. And some of the very narrow strips are areas that are not covered by any ink. The uniformity of the ink is a great factor impacting the conductivity. Thus, the portions and the average color intensity of the single, double layer ink areas, and no ink areas are meaningful features in predicting sheet resistance.

First step of the segmentation is to separate the electrode area and the background area (Fig. 2.15). The flat field corrected RGB images are converted to grayscale images. Sobel edge detector [8] and Otsu's method [9] are applied to the grayscale images sequentially. The background and the electrode area is cropped with the most outer edge pixels shown in image [3] of Fig. 2.15.

Then, in order to do segmentation in the electrode area, Otsu's method is applied to the background masked grayscale image. Thus, the resulting image [5] in Fig.

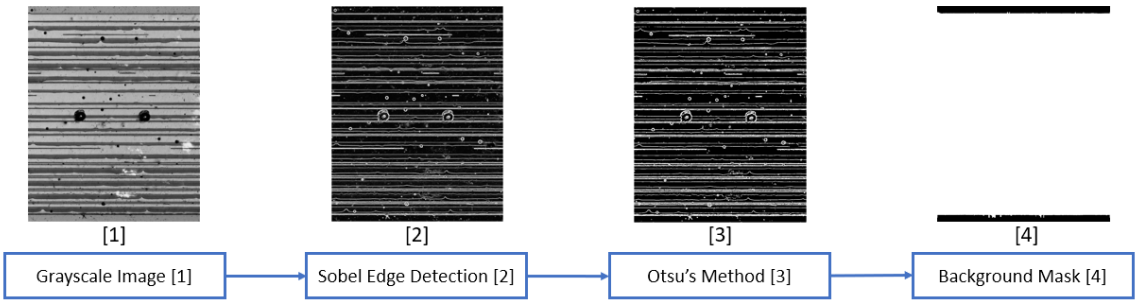

Fig. 2.15. Background Subtraction

2.16 separates the single layer ink area and other areas. For subtracting the single layer ink area and background area, the resulting image from the last step ([5] in Fig. 2.16) is inverted and masked with a background mask. K-mean clustering [10] [11] training method is applied to the pixels of the inverted and masked image. Pixels are grouped into 3 clusters based on their pixel values ([6] in Fig. 2.16). The connected components are considered as double layered ink areas or no ink areas according to their pixel distribution in 3 clusters. The final segmentation result is shown [7] in Fig. 2.16. Comparing [7] in Fig. 2.16 and the RGB image, the single layer, double layer, and no ink area are segmented correctly, except the strip located in the center is mistakenly segmented as no ink area which is affected by the circle dents left by the sheet resistance measurement probe heads.

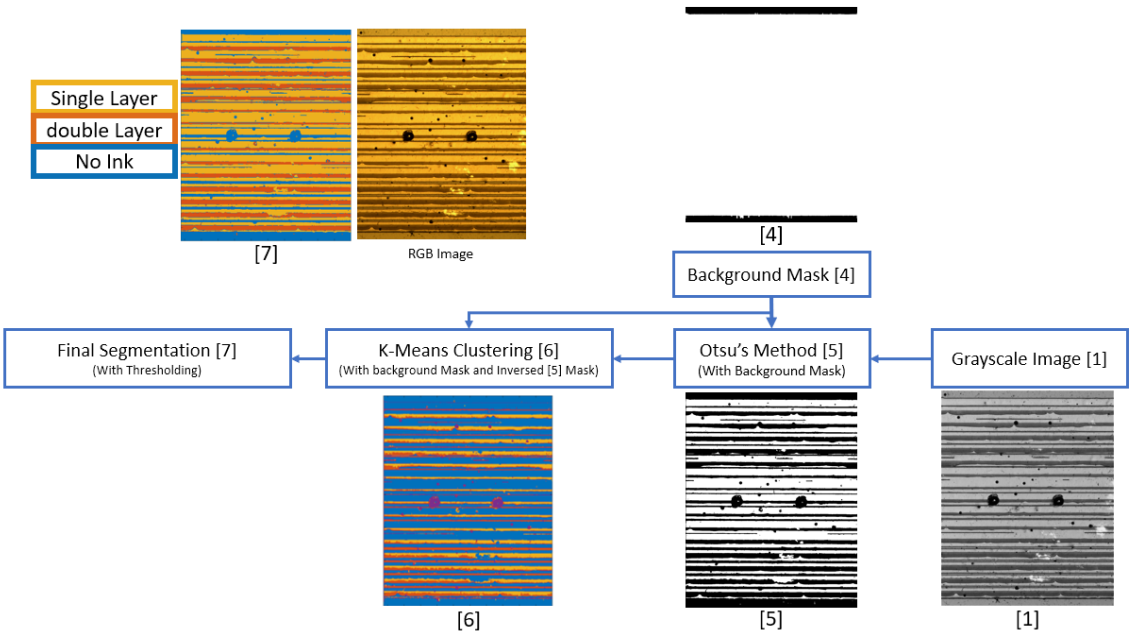

Fig. 2.16. Image Segmentation Process

After the segmentation, the proportions of each segmentation area over the electrode area is calculated based on the image [7] in Fig. 2.16 and the average light intensity for each segmentation area is calculated based on both the image [7] in Fig. 2.16 and the Y values, which represents the relative luminance for each pixel, of the flat field corrected image in XYZ color space [12].

As specified in the document of the light source, the color temperature reaches 3250 K when the intensity is set to maximum. However, when capturing the images, the intensity failed to set to its maximum. The white point used here for transforming from RGB color space to XYZ space is (0.44757, 0.40745) for 2856 K color temperature [13]. Since no gamma correction is applied, the raw RGB values are linearized value. RGB color space images are converted to XYZ color space using the formula below (Equation 2.2).

$$\begin{bmatrix} X \\ Y \\ Z \end{bmatrix} = M \begin{bmatrix} R \\ G \\ B \end{bmatrix}$$

For calculating transforming matrix M :

$$\frac{1}{WP_y} \begin{bmatrix} WP_x \\ WP_y \\ WP_z \end{bmatrix} = \begin{bmatrix} x_r & y_r & z_r \\ x_g & y_g & z_g \\ x_b & y_b & z_b \end{bmatrix} \begin{bmatrix} \alpha_1 \\ \alpha_2 \\ \alpha_3 \end{bmatrix}$$

$$M = \begin{bmatrix} x_r & y_r & z_r \\ x_g & y_g & z_g \\ x_b & y_b & z_b \end{bmatrix} \begin{bmatrix} \alpha_1 & 0 & 0 \\ 0 & \alpha_2 & 0 \\ 0 & 0 & \alpha_3 \end{bmatrix} \tag{2.2}$$

where $\begin{bmatrix} WP_x \\ WP_y \\ WP_z \end{bmatrix}$ *is white point matrix,*

$\begin{bmatrix} x_r & y_r & z_r \\ x_g & y_g & z_g \\ x_b & y_b & z_b \end{bmatrix}$ *is RGB standard color primaries.* [14]

Edge Raggedness Of Printed Strips

The edge raggedness of the electrode's top and bottom edges are calculated, which are specified in the background mask image ([4] in Fig. 2.15 or Fig. 2.16). The edge raggedness is the geometric distortion of an edge from ideal. Simple linear regression is applied to the positions of the edge pixels to form a fitted line. The raggedness is calculated as the standard deviation of the residuals of the actual contour to the fitted line [15] (Equation 2.3).

$$Edge\ Roughness(ER) = \sqrt{\frac{1}{m \times n} \sum_{i=1}^{m} \sum_{j=1}^{n} \left[Fitted\ line(i,j) - Data(i,j) \right]^2}, \tag{2.3}$$

$$where \quad m = image\ width,\ n = image\ length,\ (i,j) = Pixel\ Position$$

Surface Roughness

Multiple assessment methods from various aspects to describing surface roughness are generated and performed. The most straight forward one among these methods is the edge proportion (EP) method. Edge proportion is the ratio of edge pixels to the total pixels in the electrode area (Equation 2.4). So, this EP is calculated based on the binary image [3] and [4] in Fig. 2.15.

$$\begin{aligned} Edge\ Proportion(EP) &= \frac{No.\ of\ Edge\ Pixels}{No.\ of\ Total\ Pixels\ in\ Electrode\ Area} \\ &= \frac{\sum_{i=1}^{m} \sum_{j=1}^{n} Image[3](i,j)}{\sum_{i=1}^{m} \sum_{j=1}^{n} Image[4](i,j)} \end{aligned}$$

$$where \quad m = image\ width,\ n = image\ length,\ (i,j) = Pixel\ Position$$

$$Image[3]\ and\ Image[4]\ are\ binary\ image\ [3]\ and\ [4]\ from\ Fig.2.15. \tag{2.4}$$

Since the light intensity is fixed and the images are taken right on top of the targeted area, standard deviation of the Y values (representing the relative luminance for each pixels) of the image in CIEXYZ [12] space is chosen to be one of the surface roughness measuring parameter. Unevenness structures can appear with any dimen-

sions and it is hard to justify whether a deep pinhole or a big but shallow dent is with larger roughness or has more impact on the sheet resistance measurement. With the Gaussian pyramid [16] technique, the surface roughness with variety scales can be collected. As shown in Fig. 2.17, the original image is the layer 0 in the Gaussian pyramid. The layer 0 image is filtered with a Gaussian filter and then downsampled to layer 1 resulting in half size along each spacial dimension. The same operation is applied to layer 1 image to produce the layer 2 image and to layer 2 image to produce the layer 3 image. Then, all the images of all the layers are upsampled to the same size of the layer 0 image using linear bilateral interpolation. Standard deviation of the Y values of the upsampled images belonging to each layer of Gaussian pyramid is calculated (Equation 2.5).

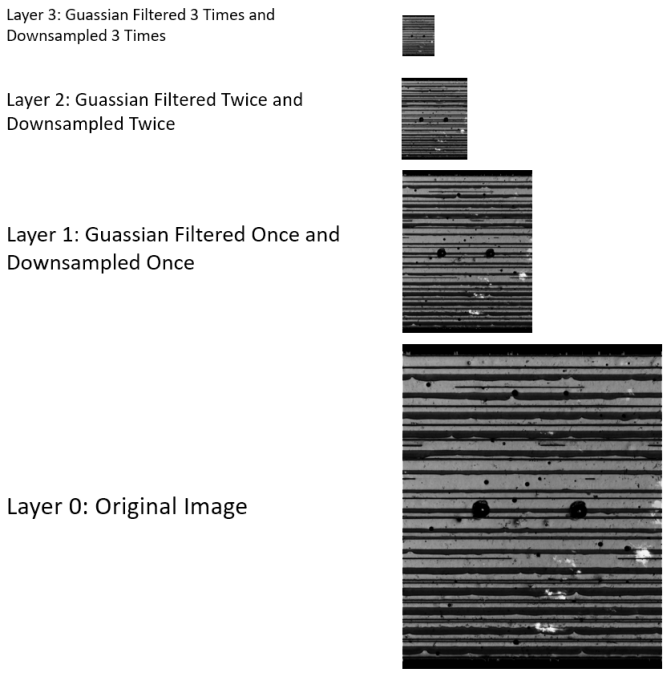

Fig. 2.17. Gaussian Pyramid

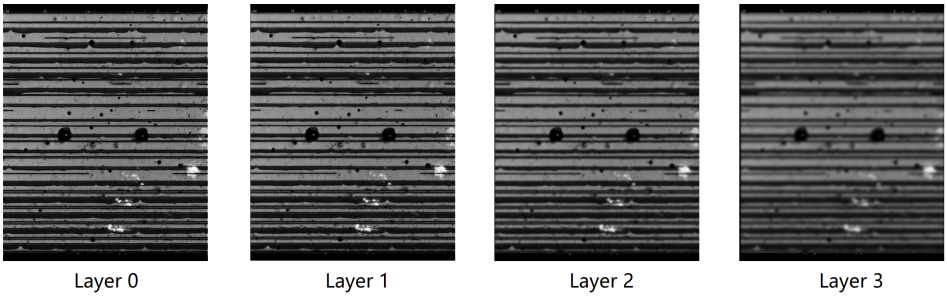

Fig. 2.18. Upsampled Images of Gaussian Pyramid

$$Surface\ Roughness\ with\ GP = \sqrt{\frac{\sum_{i=1}^{m}\sum_{j=1}^{n}(Y(i,j)-\bar{Y})}{M \times N - 1}} \tag{2.5}$$

$$where \quad m = image\ width,\ n = image\ length,\ (i,j) = Pixel\ Position$$

Another technique called local binary pattern [17] (LBP) is well known for its light dependency and wide applications in characterizing texturing of paper [18] and computer vision area for face detection [19]. This technique is also applied here for providing more information about the printed electrode surface. The local binary pattern used here is rotation invariant method with circular operators. With this method, the output of the local binary pattern with eight neighbours is a 10-element array to represent the local texture.

2.2.2 Model Fitting

All the features extracted from images of the Inkjet printed silver electrodes are merged into one matrix with total 19 columns and 600 rows as an input matrix for the training model. The input matrix contains five columns for the image segmentation, 14 columns for surface roughness. Since 20 electrodes are printed for totally six sets of printing parameters and each electrodes have five sheet resistance measurement and five matched images, total number of rows for the input matrix sums to 600. For the same reason, the output matrix which is the sheet resistance measurement data

for each measuring position is also with 600 rows. For data with one set of printing parameters, one model is trained. In total, six models are trained.

Data Normalization

Before the model fitting process, all of the data need to be normalized. After normalization, all the data is scaled to the range from 0 to 1. All of the feature extracted from images is normalized with Min-Max Normalization method and the sheet resistance measurement data is normalized with logarithm normalization method (Equation 2.6).

$$\begin{aligned} Data &= \frac{Data - min(Data)}{max(Data) - min(Data)} \\ R_u &= \frac{log_{10}R}{log_{10}[]max(R)]} \end{aligned} \tag{2.6}$$

Training Models Comparison

Two regression training models has been tested separately for the model fitting process: least square [20] [21] (LSQR) method and the support vector machine regression [22] [23] (SVM Regression) method. Both the least square regression method and the support vector machine regression method is trained with all the data and tested on the same data. The result directly output from the test procedure is the predicted sheet resistance according to the features extracted from images. The average of the five experimental sheet resistance measurements for each electrodes ($\bar{R}_{Exp}$) is calculated to represent the print quality for the whole electrode. And the average of the five predicted sheet resistance ($\bar{R}_{Pred}$) is calculated in the same way.

All the data (including the sheet resistance measurement data) are normalized to range of [0,1] before training and testing process. The RMSE (%) on normalized data in the Table 2.2. listed below is calculated with the normalized sheet resistance. Both of the measured sheet resistances and the predicted sheet resistances are re-scaled to

Table 2.2.
Model Fitting Results

Drop Size **10/1 pL**	**Drop Space** μ**m**	**RMSE (%) For LSQR**		**RMSE (%) For SVM Regression**	
		Normalized	**Re-scaled**	**Normalized**	**Re-scaled**
10 pL	40	1.63	15.49	2.16	20.00
	25	5.14	36.30	6.58	40.55
	20	1.31	7.45	2.21	11.54
1 pL	25	1.02	8.98	1.21	10.93
	20	3.61	28.91	5.68	38.83
	10	1.94	11.03	3.10	20.56
Average		**2.83**	**21.02**	**4.00**	**26.55**

original scale. The RMSE (%) on re-scaled data is calculated with the sheet resistance data that are re-scaled to the original scale of data.

Root mean square error (RMSE) in percentage is used here for evaluate the degree of fitting for both of the regression training models. The calculation of RMSE in percentage is based on the average experimental sheet resistance measurements ($\bar{R}_{Exp}$) and the average predicted sheet resistance for each electrodes ($\bar{R}_{Pred}$) (Equation 2.7).

$$RMSE\,(\%) = \sqrt{\frac{1}{N}\sum_{index=1}^{N}\left[\frac{|\,\bar{R}_{Pred}(index) - \bar{R}_{Exp}(index)\,|}{\bar{R}_{Exp}(index)}\right]^2} \times\ 100\% \qquad (2.7)$$

$$where \quad N = total\ No.\ of\ electrodes$$

Table 2.2 shows the RMSE in percentage for both of the regression models.

2.2.3 N-Fold Cross-Validation

A five-fold cross validation is performed to assess the prediction accuracy of the models. For one test, the 120 electrodes are divided into five groups randomly. Every group has four electrodes that are printed with the same set of parameters. With six sets of printing parameters, the number of electrodes for each group sums to 24. Every one group is served as a test set and the rest of the groups are the training set. Then, the 120 electrodes is reformed randomly into five groups serving for next test. The total number of test iterations is 50 times, which means the 120 electrodes are reformed for 100 times and every electrodes is tested 100 times. The final test error for each electrode is the average value across the 100 tests. Because the final test error for each page is based on multiple repetitions of the training process with randomly formed data sets, the final test error is also called average absolute relative error (Avg.Abs.Re.Error). Fig. 2.19 and Fig. 2.21 listed below show the average absolute relative error for 120 electrodes with different training models.

$$Avg.Abs.Re.Error\ (\%) = \frac{\sum_{t=1}^{T} Error(t)}{T} \times 100\%$$
$$where \quad Error(t) = \frac{\mid R_{Pred} - R_{Exp} \mid}{R_{Exp}}, \quad t = index\ of\ test,\ T = total\ No.\ of\ tests \tag{2.8}$$

The sheet resistances are trained and tested with normalized data and the errors are also calculated based on the normalized data. The predicted sheet resistance is re-scaled back to the original data scale and the error is recalculated based on the original experimental sheet resistance measurements and the re-scaled predicted sheet resistance. Table 2.3 and figures (from Fig. 2.18 to Fig. 2.21) listed below show the recalculated error.

Table 2.3.
5-Fold Cross Validation Results Comparison Between LSQR and SVM Regression Methods.

%	LSQR Regression	SVM Regression
Average	25.77	25.48
Max	123.07	126.51
Min	0.03	0.29
STDEV	26.30	26.75

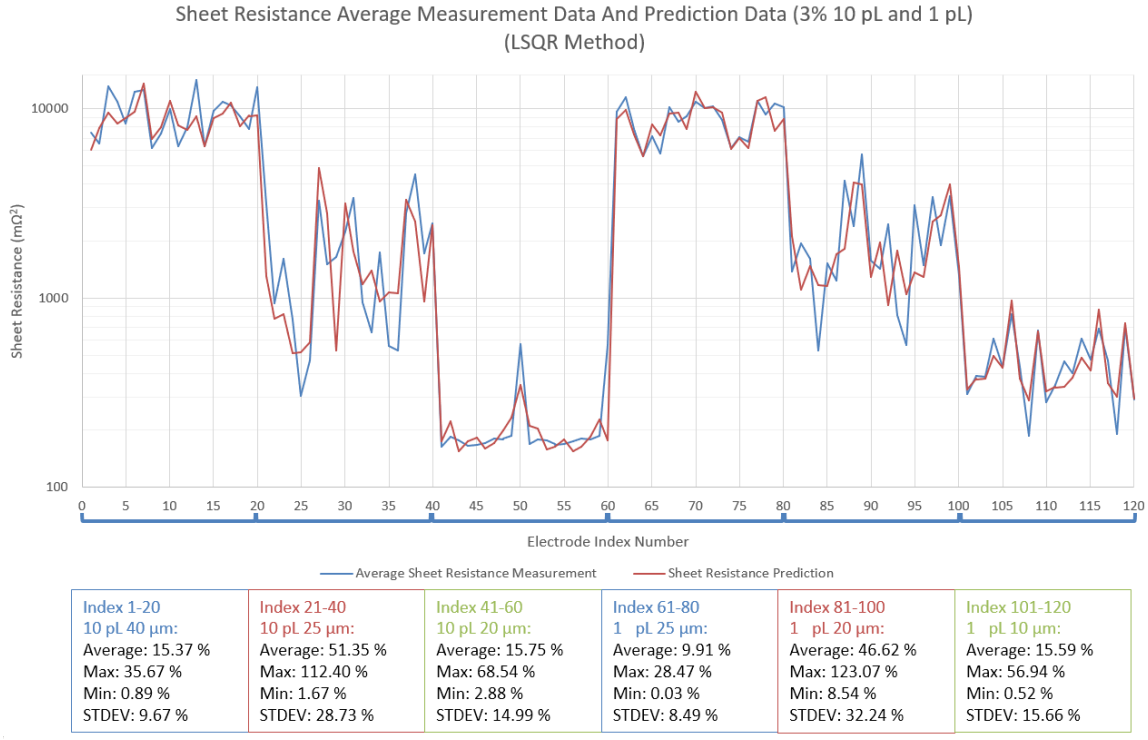

Fig. 2.19. Cross-Validation Trained and Tested with Least Square Method: Original Experimental and Re-scaled Predicted Sheet Resistance

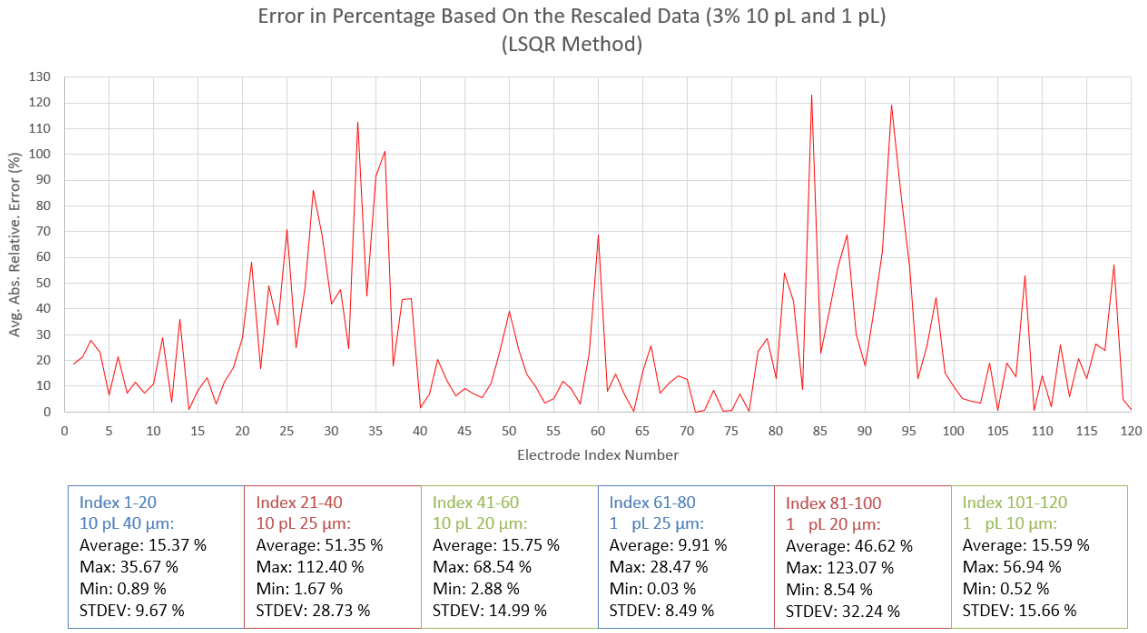

Fig. 2.20. Cross-Validation Trained and Tested with Least Square Method: Error Calculated with Original Experimental and Re-scaled Predicted Sheet Resistance

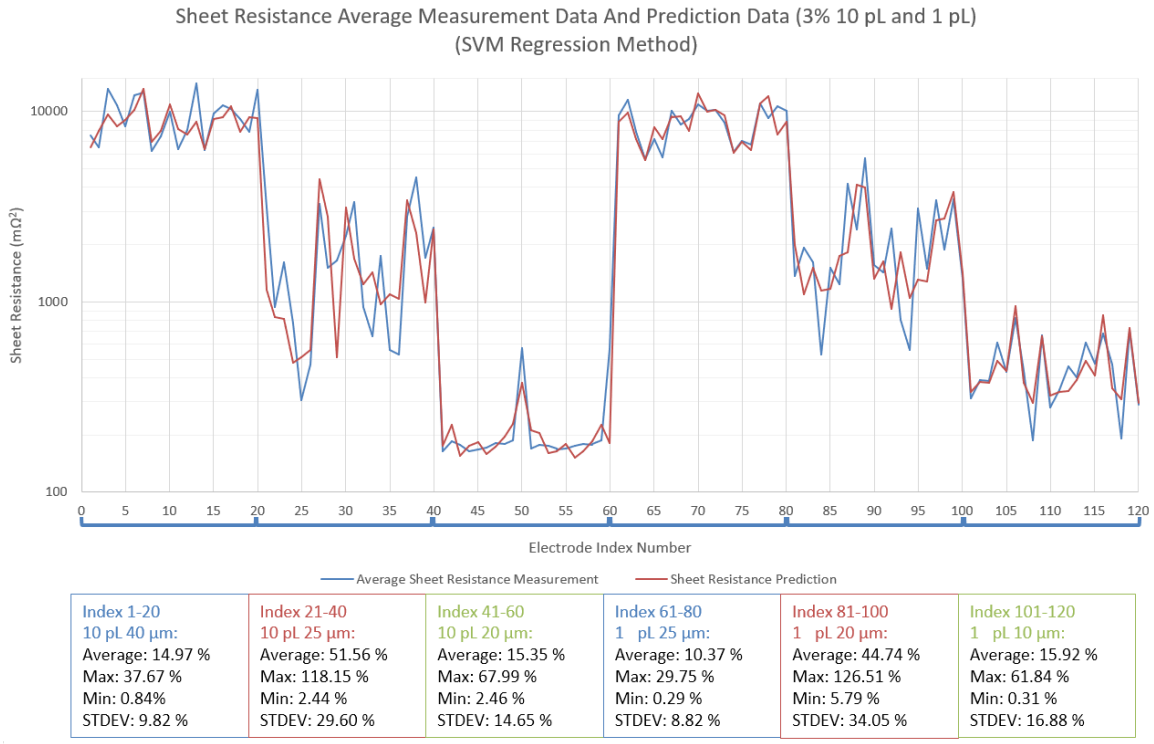

Fig. 2.21. Cross-Validation Trained and Tested with SVM Regression Method: Original Experimental and Re-scaled Predicted Sheet Resistance

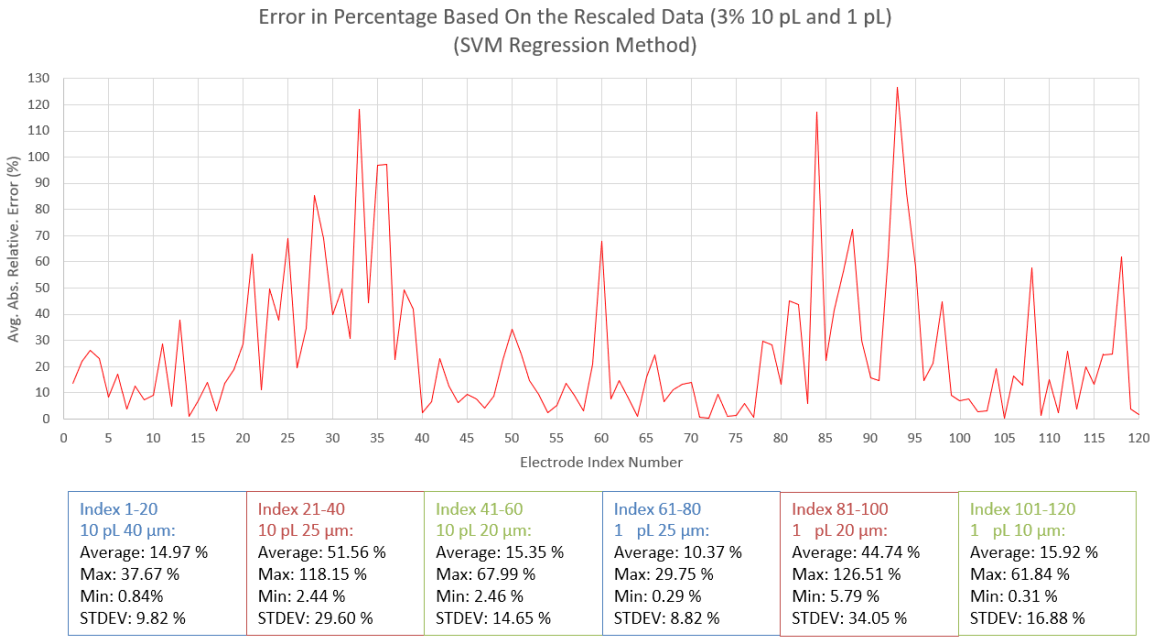

Fig. 2.22. Cross-Validation Trained and Tested with SVM Regression Method: Error Calculated with Original Experimental and Re-scaled Predicted Sheet Resistance

2.2.4 Acceptable Sensors Prediction Results Based On Sheet Resistance Data

Judging the acceptable sensors is vital based on the prediction module mentioned in previous sections. It is defined that the acceptable electrodes are the electrodes with the sheet resistance values ranged within 1.5 standard deviation based on the measured sheet resistance data. The predicted acceptable electrodes are the electrodes with the sheet resistance values ranged within 1.5 standard deviation based on the predicted sheet resistance data.

Based on the module introduced in previous section, the prediction of the acceptable electrodes is as accurate as 87%.

3. SUMMARY

From results shown for the five-fold cross-validation, for either least-square regression or SVM regression, the average absolute relative error ranges from 0% to 120%. The sheet resistance measurements are normalized using logarithm method which causes higher degree of compression. Thus, although both of the models result in errors ranging from 10% to 39% in the model fitting process, the error in the five-fold cross-validation are much greater than they appear in model fitting process.

In spite of this, this image-based and non-contact method is novel and in-situ friendly. Once the training model is trained, no more sheet resistance measurements are needed. With the imaging system set up to the output of the printer, sheet resistance can be predicted and quality of printed electrodes can be assessed.

Considering the main purpose of sheet resistance prediction is evaluating the quality of Inkjet printed electrodes, determining whether the quality of the printing job is acceptable or not is much more essential compared to the accuracy of the sheet resistance measurement. A further step for this investigation can be to set a threshold range regarding the features extracted from the images of the Inkjet printed electrodes and judge whether the electrode is acceptable.

4. FOLLOW-UP WORK FOR TONER USAGE PREDICTION

Lately, as laser electro-phorographic printers have become common tools and widely implemented in every office. The prediction of toner usage is valuable technique for customers, especially in condition where the cost of toner cartridges have become a crucial part in economic decisions and purchase behaviors.

The overall structure of the two-stage method for toner usage prediction studied by Wang [24], Ju [25], and Gao [26] is shown in Fig. 4.1. below. The method is time-consuming and data storage demanding. Thus, one of the focuses of this follow-up work is to prune and simplify the process. Since the previous work only examined the prediction accuracy on black (K) ink cartridge, this follow-up work further includes the test results of the toner usage prediction on cyan (C), magenta (M), and yellow (Y) ink cartridges.

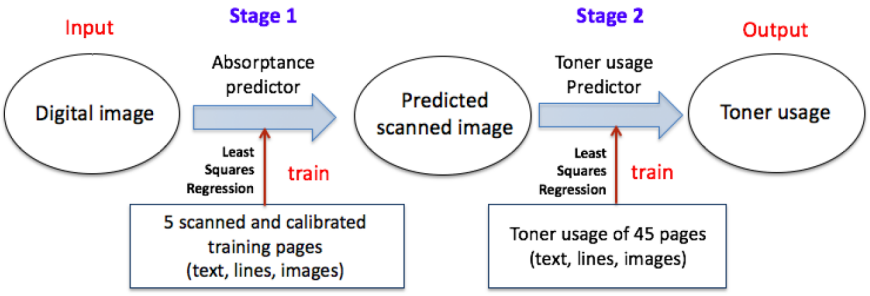

Fig. 4.1. Overall Structure of the Two-Stage Method

4.1 Training Page Redesign For Stage One

As shown in the overall structure of the two-stage method (Fig. 4.1.), for the first stage, five printed images (Fig. 4.2) need to be scanned. For the previous work, they are all scanned with scanning resolution of 1800 dpi. Every scanning takes around 30 minutes. The decoding of the fiducial marks in scanned digital images costs about two hours and the stage one training process is too demanding on memory and cannot run on a average home computer.

Fig. 4.2. Five Training Pages for Stage One

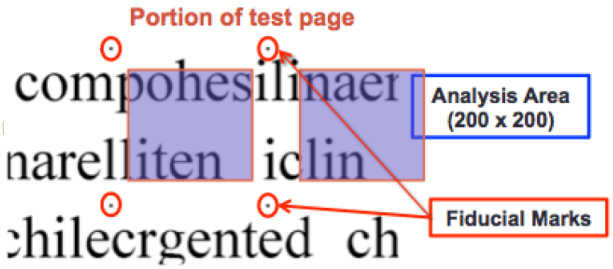

Fig. 4.3. Five Training Pages for Stage One

The five images is shown in Fig. 4.2. Before training process, the fiducial marks are added on the images and then printed. And the analysis area as shown in Fig. 4.3. are specified by the fiducial marks. The area cropped by four fiducial marks are fiducial blocks. The center 200 x 200 pixels area of the fiducial blocks are analysis area.

Since the method of decoding fiducial marks for text pages and the line page is the same, we tried to mixed them together within one one page by randomly selecting equal number of fiducial blocks from the training page 1 and training page 2 as well as added horizontal and vertical line sets from training page 3 on the right and bottom side of the page. The continuous-tone images are mixed together in one page by removed half of the fiducial blocks from training page 4 and 5 and mixed the remaining. In this case, the five training page for stage one is reduced to two redesigned training pages (Fig. 4.4.). At the same time, the scanning resolution is reduced from 1800 dpi to 1200 dpi.

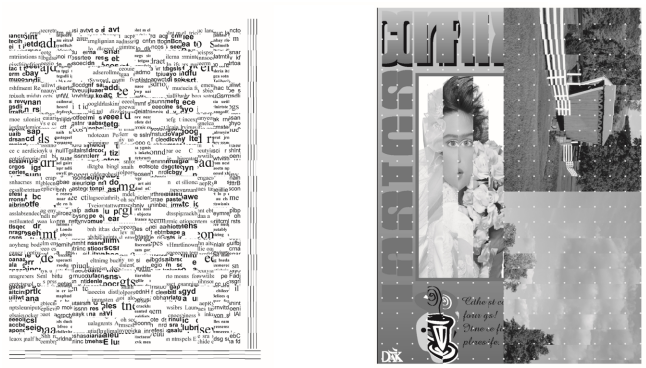

Fig. 4.4. Two Training Pages for Stage One

With all these adjustments, stage one training process can be completely on a average home computer. And time consumed and usage of memory for stage one training is largely reduced, as specified in the Table 4.1., Table 4.2., and Table 4.3 respectively.

Table 4.1.
Time Consuming Comparison Between Five-Page and Two-Page Stage One Training

Training Set	**Scanning**	**Fiducial Mark Decoding**	**Training**
Five-Page	30 Minutes×5	2 Hours	Not Runable
Two-Page	10 Minutes×2	30 Minutes	66 Hours

Table 4.2.
Memory Usage for Five-Page Stage One Training

	Used (GB)	**Buffer (MB)**	**Cached (GB)**	**Free (GB)**
Start With	39.20	628.05	90.98	121.38
Maximum Reaches	107.96	628.06	91.14	52.46
Average	84.07	628.06	91.13	76.35

Table 4.3.
Memory Usage for Two-Page Stage One Training

	Used (GB)	**Buffer (MB)**	**Cached (GB)**	**Free (GB)**
Start With	29.45	631.17	101.98	120.12
Maximum Reaches	56.91	631.17	101.98	92.65
Average	48.86	631.17	101.98	100.71

The root mean square error (RMSE) is also used as an assessment for absorptance prediction accuracy (Equation 4.1). The estimated pages are generated based on the absorptance estimation method created by Gao. Table 4.4 shows the absorptance prediction error for each of the five original training pages by using different stage one look up table (LUT) and different trained page sets (five-page set or two-page set) on black(K) ink cartridge of the same laser printer. All prediction errors are based on 255. It is obvious that the prediction accuracy of the two-page set is extremely close to the results trained with the five-page set, even the two-page set is scanned with lower scanning resolution.

$$RMSE\,(\%) = \sqrt{\frac{1}{m \times n \times l} \sum_{i=1}^{m} \sum_{j=1}^{n} \Big[predicted(i,j) - estimated(i,j) \Big]^2} \times 100\%$$
$$where \quad m = image\,width,\ n = image\,length,\ (i,j) = Pixel\ Position \tag{4.1}$$

Table 4.4.
Absorptance Prediction Error, Comparison between the five-page set and two-page set

	RMSE (%)					
Page No.	**Original LUT**		**LUT (Method 1)**		**LUT (Method 2)**	
	Five-Page (1800 dpi)	**Two-Page (1200 dpi)**	**Five-Page (1800 dpi)**	**Two-Page (1200 dpi)**	**Five-Page (1800 dpi)**	**Two-Page (1200 dpi)**
1	6.48	6.32	6.81	6.74	7.04	6.95
2	6.69	6.50	7.09	7.00	7.27	7.14
3	7.09	6.84	7.68	7.52	7.92	7.78
4	4.20	4.14	4.28	4.22	4.29	4.24
5	4.24	4.24	4.26	4.26	4.28	4.29
Average	**5.74**	**5.61**	**5.82**	**5.95**	**6.16**	**6.08**

4.2 Stage Two Results for Different Color of Ink

For stage two, toner usage prediction is mapped from the absorptance predictions of stage one by a toner usage predictor. The toner usage predictor was built with 45 assorted images shown in the Fig. 4.5. In order to save labour and time, the total page number used for stage two training is eliminated to 26 pages, which is also shown in the Fig. 4.5.

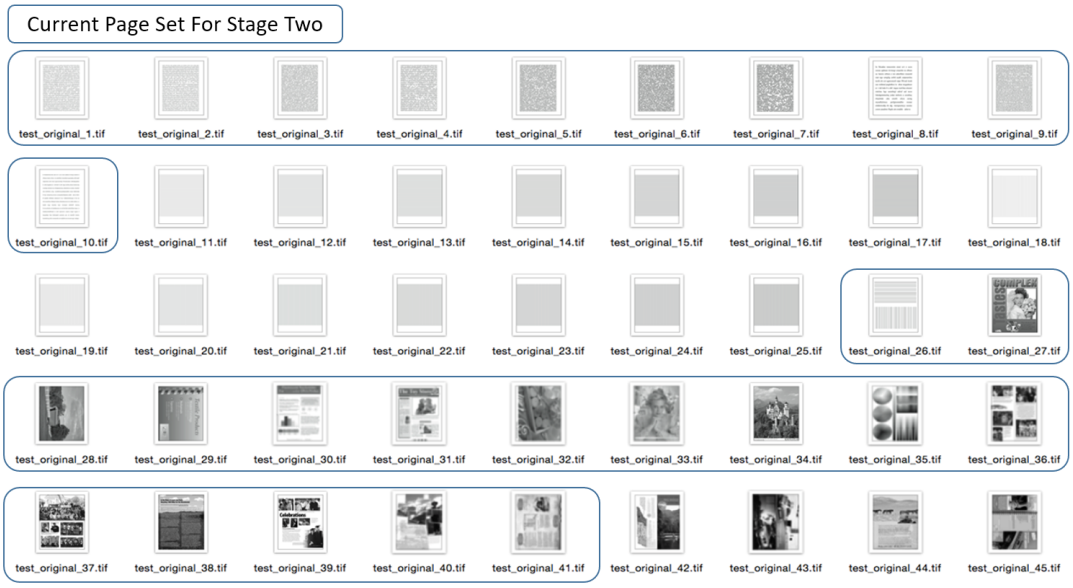

Fig. 4.5. Current Page Set for Stage Two

Following instructions mentioned by Gao [26], toner usage measurements for all pages in the new page set for stage two has been conducted on black ink cartridge, cyan ink cartridge, magenta ink cartrdge, and yellow ink cartridge separately. In other words, each 26 images are printed 100 pages with black ink only.The weight of the toner cartridge is been taken before and after printing each set of 100 pages. The same procedures are applied to printing the images with cyan, magenta, and yellow ink. The final training results for stage two on every color cartridges are shown in figures from Fig. 4.6 to Fig. 4.9 below.

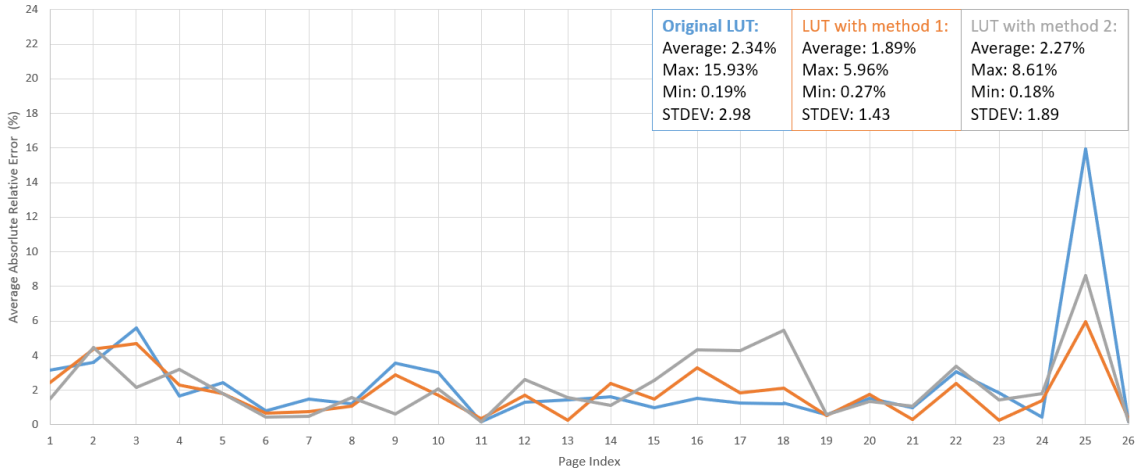

Page Index Reference: index from 1 to 10 are text pages,
index 11 is a line page with horizontal and vertical lines of various width
index from 12 to 26 are continuous-tone image pages

Fig. 4.6. Stage Two: Toner Usage Prediction Error On Color Cyan Cartridge

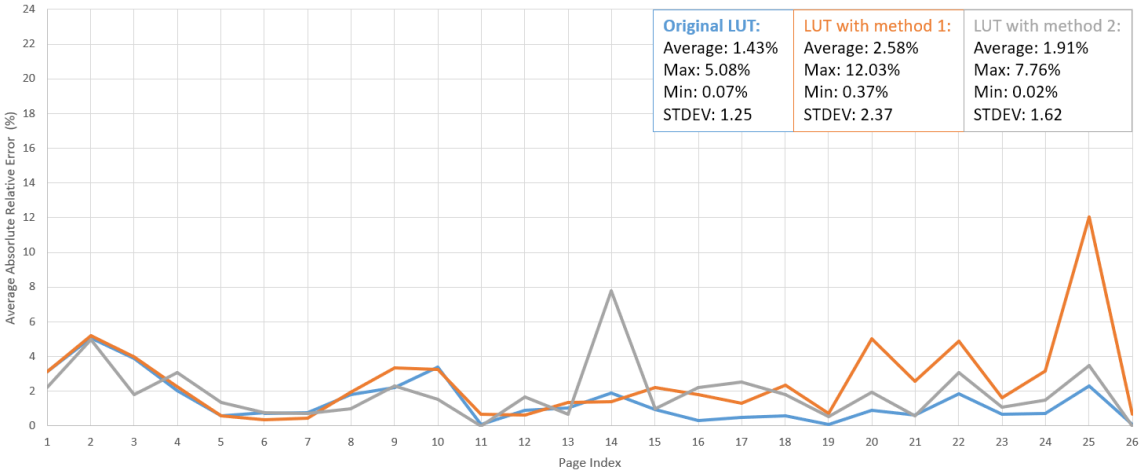

Page Index Reference: index from 1 to 10 are text pages,
index 11 is a line page with horizontal and vertical lines of various width
index from 12 to 26 are continuous-tone image pages

Fig. 4.7. Stage Two: Toner Usage Prediction Error On Color Magenta Cartridge

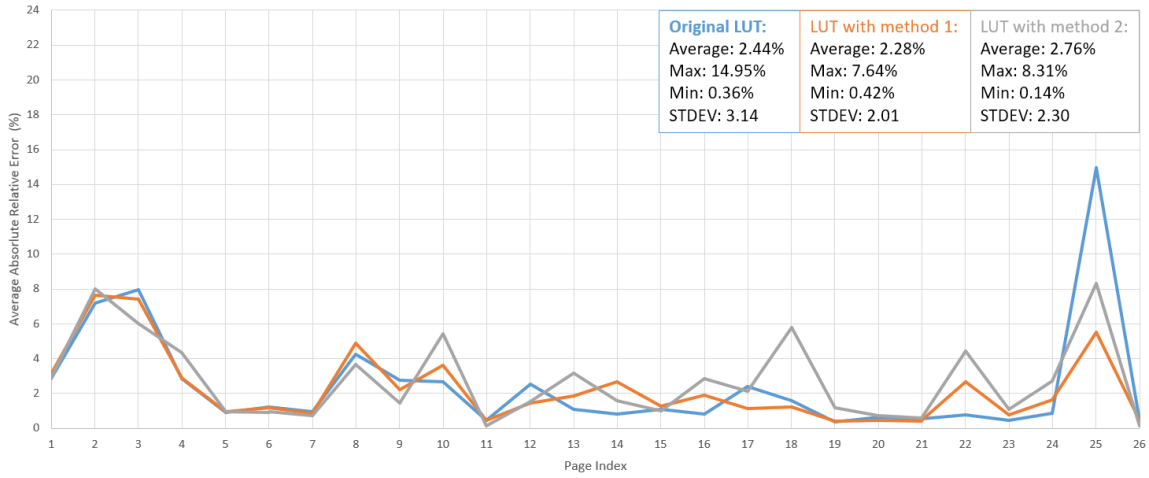

Page Index Reference: index from 1 to 10 are text pages,
index 11 is a line page with horizontal and vertical lines of various width
index from 12 to 26 are continuous-tone image pages

Fig. 4.8. Stage Two: Toner Usage Prediction Error On Color Yellow Cartridge

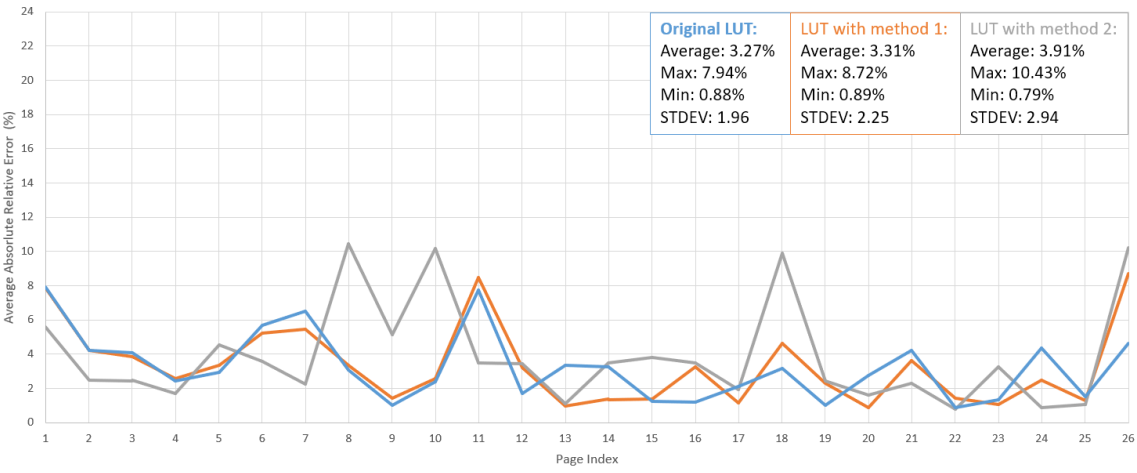

Page Index Reference: index from 1 to 10 are text pages,
index 11 is a line page with horizontal and vertical lines of various width
index from 12 to 26 are continuous-tone image pages

Fig. 4.9. Stage Two: Toner Usage Prediction Error On Color Black Cartridge

4.3 Summary for Follow-Up Work of Toner Usage Prediction

The follow-up work of toner usage prediction validates the method improved by Gao [26] and can be perfectly applied to not only the black color cartridges but also all the rest of the printing color cartridges. The printer used for this follow-up work is not the same model as the ones Gao did experiments with. Thus, in some scales, the method has a wide applicability across various laser electro-phorographic printer models on every printing color catridges.

If needed, an investigation can be performed on absorptance estimation accuracy variation with different percentage that toner remaining in the cartridge.

REFERENCES

REFERENCES

[1] E. S. Park, Y. Chen, T.-J. K. Liu, and V. Subramanian, "A new switching device for printed electronics: Inkjet-printed microelectromechanical relay," *Nano Letters*, vol. 13, no. 11, pp. 5355–5360, 2013.

[2] B.-J. Kim, H.-J. Kim, S.-M. Jung, Y.-H. Kim, S. Ha, T.-S. Yoon, and H. H. Lee, "Capacitance–voltage characteristics of metal-polymer-silicon device with inkjet-printed ag electrode," *Thin Solid Films*, vol. 519, no. 13, pp. 4319–4323, 2011.

[3] H. Han, P. S. Amegadze, J. Park, K.-J. Baeg, and Y.-Y. Noh, "Effect of gate electrode conductivity on operation frequency of inkjet-printed complementary polymer ring oscillators," *Thin Solid Films*, vol. 546, pp. 141–146, 2013.

[4] J. H. Choi, K. Ryu, K. Park, and S.-J. Moon, "Thermal conductivity estimation of inkjet-printed silver nanoparticle ink during continuous wave laser sintering," *International Journal of Heat and Mass Transfer*, vol. 85, pp. 904–909, 2015.

[5] K.-C. Chung, H.-N. Cho, M.-S. Gong, Y.-S. Han, J.-B. Park, D.-H. Nam, S.-Y. Uhm, and Y.-K. Seo, "Organic silver complexes, their preparation methods and their methods for forming thin layers," Jul. 24 2012, US Patent 8,226,755.

[6] FUJI, "Dimatix material printer," https://www.fujifilmusa.com/shared/bin/dimatix_materials_printer_dmp-2850.pdf, 2016.

[7] J. A. Seibert, J. M. Boone, and K. K. Lindfors, "Flat-field correction technique for digital detectors," in *Medical Imaging 1998: Physics of Medical Imaging*, vol. 3336. International Society for Optics and Photonics, 1998, pp. 348–355.

[8] O. R. Vincent, O. Folorunso *et al.*, "A descriptive algorithm for sobel image edge detection," in *Proceedings of Informing Science & IT Education Conference (InSITE)*, vol. 40. Informing Science Institute California, 2009, pp. 97–107.

[9] N. Otsu, "A threshold selection method from gray-level histograms," *IEEE Transactions On Systems, Man, and Cybernetics*, vol. 9, no. 1, pp. 62–66, 1979.

[10] D. Arthur and S. Vassilvitskii, "k-means++: The advantages of careful seeding," in *Proceedings of the Eighteenth Annual ACM-SIAM Symposium on Discrete Algorithms*. Society for Industrial and Applied Mathematics, 2007, pp. 1027–1035.

[11] S. Lloyd, "Least squares quantization in PCM," *IEEE Transactions On Information Theory*, vol. 28, no. 2, pp. 129–137, 1982.

[12] H. S. Fairman, M. H. Brill, and H. Hemmendinger, "How the CIE 1931 color-matching functions were derived from Wright-Guild data," *Color Research & Application: Endorsed by Inter-Society Color Council, The Colour Group (Great Britain), Canadian Society for Color, Color Science Association of Japan, Dutch Society for the Study of Color, The Swedish Colour Centre Foundation, Colour Society of Australia, Centre Français de la Couleur*, vol. 22, no. 1, pp. 11–23, 1997.

[13] J. Schanda and M. Danyi, "Correlated Color-Temperature Calculations in the CIE 1976 chromaticity diagram," *Color Research & Application*, vol. 2, no. 4, pp. 161–163, 1977.

[14] J. Schanda, *Colorimetry: Understanding the CIE System.* John Wiley & Sons, 2007.

[15] J. Grice and J. P. Allebach, "The print quality toolkit: an integrated print quality assessment tool," *Journal of Imaging Science and Technology*, vol. 43, no. 2, pp. 187–199, 1999.

[16] E. H. Adelson, C. H. Anderson, J. R. Bergen, P. J. Burt, and J. M. Ogden, "Pyramid methods in image processing," *RCA Engineer*, vol. 29, no. 6, pp. 33–41, 1984.

[17] T. Ojala, M. Pietikäinen, and T. Mäenpää, "Multiresolution gray-scale and rotation invariant texture classification with local binary patterns," *IEEE Transactions on Pattern Analysis & Machine Intelligence*, no. 7, pp. 971–987, 2002.

[18] M. Turtinen, M. Pietikäinen, O. Silvén, T. Mäenpää, and M. Niskanen, "Paper characterisation by texture using visualisation-based training," *The International Journal of Advanced Manufacturing Technology*, vol. 22, no. 11-12, pp. 890–898, 2003.

[19] T. Ahonen, A. Hadid, and M. Pietikäinen, "Face recognition with local binary patterns," in *European Conference On Computer Vision.* Springer, 2004, pp. 469–481.

[20] C. C. Paige and M. A. Saunders, "Lsqr: An algorithm for sparse linear equations and sparse least squares," *ACM Transactions on Mathematical Software (TOMS)*, vol. 8, no. 1, pp. 43–71, 1982.

[21] R. Barrett, M. W. Berry, T. F. Chan, J. Demmel, J. Donato, J. Dongarra, V. Eijkhout, R. Pozo, C. Romine, and H. Van der Vorst, *Templates For The Solution Of Linear Systems: Building Blocks For Iterative Methods.* SIAM, 1994, vol. 43.

[22] R.-E. Fan, P.-H. Chen, and C.-J. Lin, "Working set selection using second order information for training support vector machines," *Journal Of Machine Learning Research*, vol. 6, no. Dec, pp. 1889–1918, 2005.

[23] V. Kecman, T.-M. Huang, and M. Vogt, "Iterative single data algorithm for training kernel machines from huge data sets: Theory and performance," in *Support Vector Machines: Theory and Applications.* Springer, 2005, pp. 255–274.

[24] L. Wang, D. Abramsohn, T. Ives, M. Shaw, and J. Allebach, "Estimating toner usage with laser electrophotographic printers," in *Color Imaging XVIII: Displaying, Processing, Hardcopy, and Applications*, vol. 8652. International Society for Optics and Photonics, 2013.

[25] Y. Ju, T. Kashti, T. Frank, D. Kella, D. Shaked, M. Fischer, R. Ulichney, and J. P. Allebach, "Black-box models for laser electrophotographic printers–recent progress," in *NIP & Digital Fabrication Conference*, vol. 2013, no. 1. Society for Imaging Science and Technology, 2013, pp. 66–71.

[26] M. Gao, Y. Ju, T. Nelson, T. Prenn, and J. Allebach, "Toner usage prediction for laser electrophotographic printers," in *Color Imaging XXI: Displaying, Processing, Hardcopy, and Applications*, (Part of IS&T Electronic Imaging 2016), R. Eschbach, G. G. Marcu, and A. Rizzi, Eds. San Francisco, CA, 14-18 February 2016.

APPENDICES

A. PRINTING PROCEDURES USING FUJI FILM DIMATIX

Before printing, some supplements need to be prepared and the printer need to be initially set up first. Then, a repetitive procedures can be performed for actual printing.

A.1 Supplements

The supplements include target printing figure documents, ink, substrate, and disposable packages are first need to be prepared following with following steps.

1. Using Illustrator of Adobe or any other software generates image files in bit map format with different resolutions (635 dpi for 40 μ m drop spacing, etc.) as target printing figure documents. The relations between printing resolution and printing drop spacing is indicated in Table 5 - 1 Resolutions Relationships of FUJIFILM Dimatix Materials Printer DMP-2800 Series User Manual[REF].

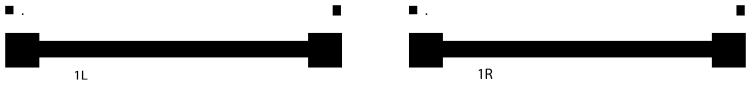

Fig. A.1. Sample for Target Printing Figure Documents

2. The silver nano-particle ink need to be mixed with Ammonium Carbamte salt in sonication bath. All the ink bottles including the original ink bottle and the ink bottles containing the mixed silver nano-particle ink with Ammonium Carbamate loading are need to be sealed with stretch and seal tape and then stored in refrigerator.

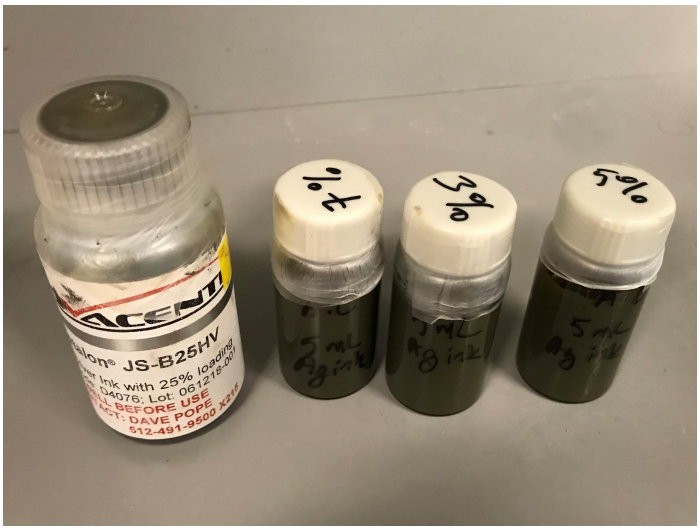

Fig. A.2. Silver Nano-Particle Ink

Fig. A.3. Printing Substrate

3. In case that more ink needed to be added to the cartridge, the secure tabs cropped with red circles in the Fig. A.4 are removed using wire cutter. Remove the white cap of the cartridge. Using a new syringe and the syringe needle from the disposable package, inject ink from ink bottle to the cartridge thought the center hole of the cartridge. After the injection, recap the cartridge with the white cap tightly.

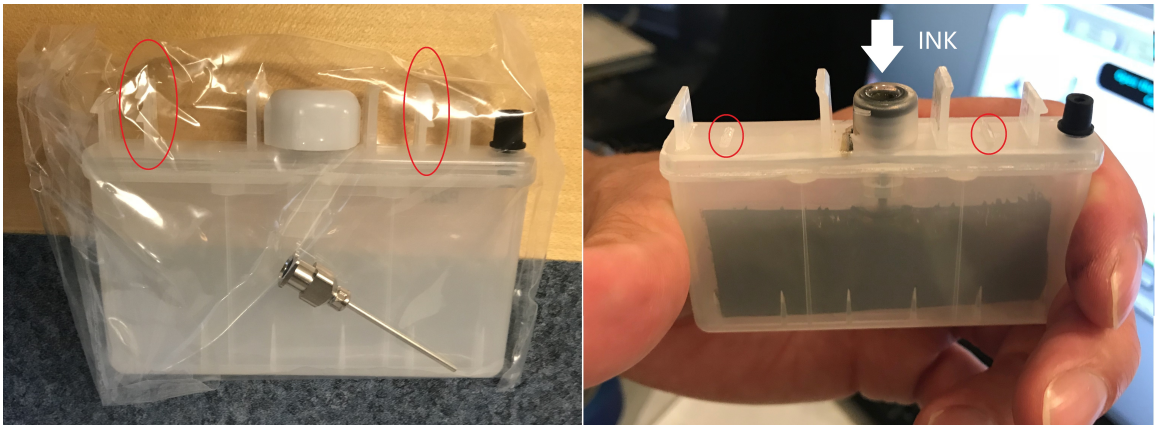

Fig. A.4. Secure Tabs Are Cut.

Fig. A.5. Dimatix Disposable Package and Other Accessories (From left to right: syringe, cleansing pad, syringe needle, cartridge with no secure tabs, and jetting model)

A.2 Setup and Print

1. Make sure the connections between the Dimatix Material printer and PC are secure and tight.

2. Turn on PC and then turn on Dimatix by switching the tab on the bottom right corner on the front of the machine (marked with red circle in Fig. A.6.).(If Dimatix is newly installed, after connecting the Dimatix with PC, turn on the PC first, allow the PC to go through the start up and then turn on Dimatix.)

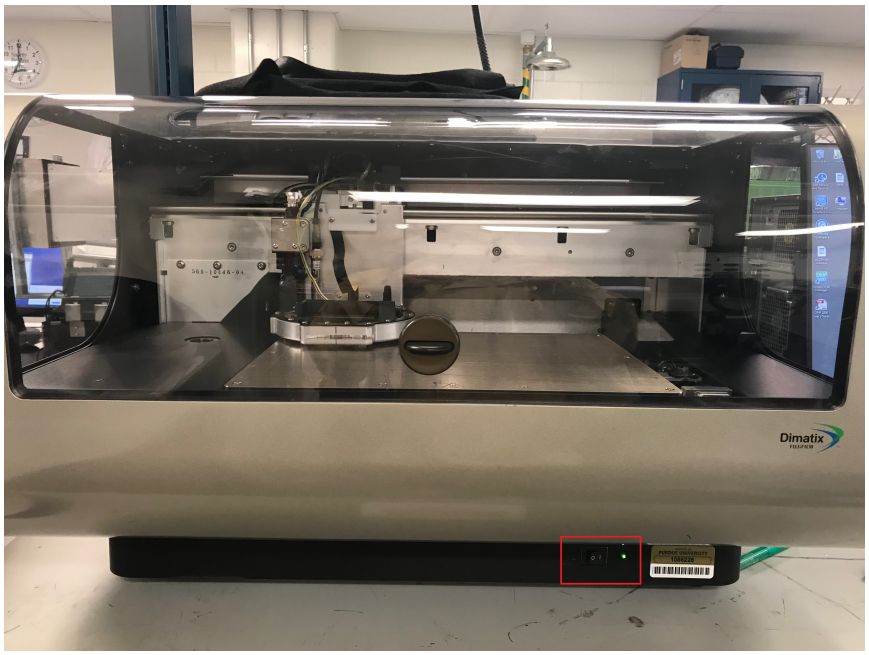

Fig. A.6. Fuji film Dimatix Matrix Printer.

3. Double click the icon named DMP 2800. Following the instructions shown on software GUI, remove anything on the platen. Remove the cap of the cartridge, assemble the cartridge with the jetting model (Parts in blue circles should match each other in Fig. A.5). An audible is heard when they are properly assembled. Using the cap of the new cleansing pad push the used cleansing pad (Fig. A.7.). The used cleansing pad will be automatically popped up. Then, install the new cleansing pad. Install the cartridge-jetting model set as shown in Fig. A.8.

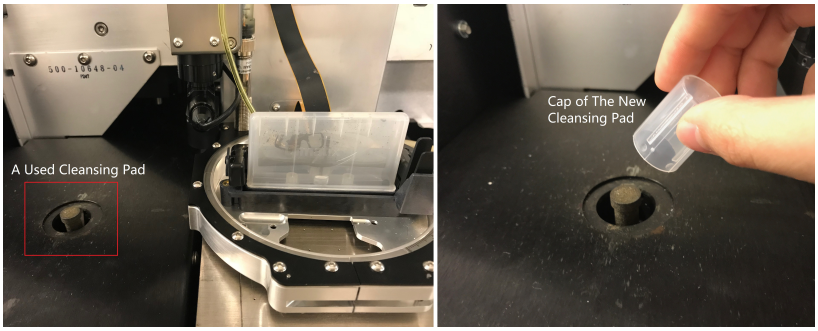

Fig. A.7. The Used Cleansing Pad Is Taken Out

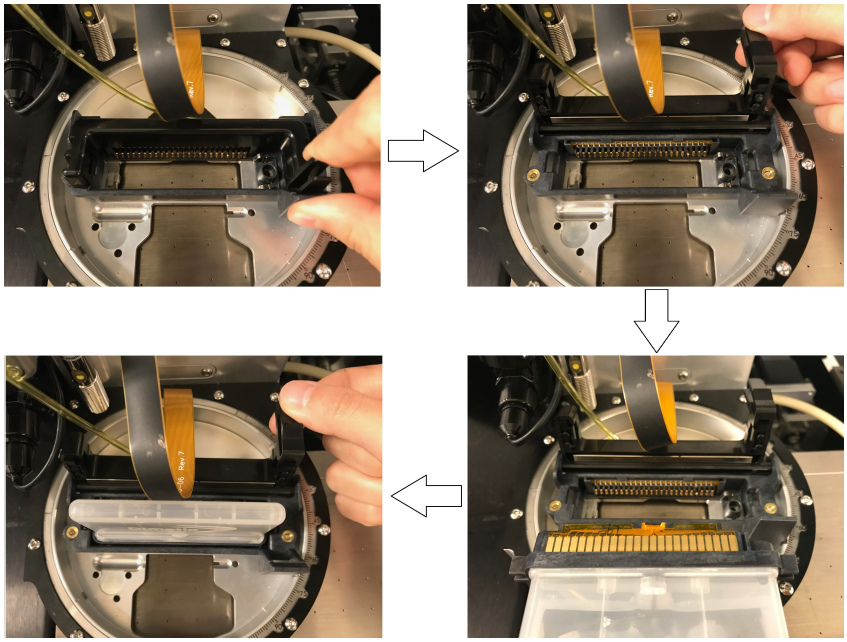

Fig. A.8. The Cartridge Is Installed

4. Following the instructions that shown on software GUI, put the substrate on the platen. In order to make sure the substrate is flat and stay in place while printing, tape the side of the substrate on the platen and turn on vacuum (Fig. A.9.).

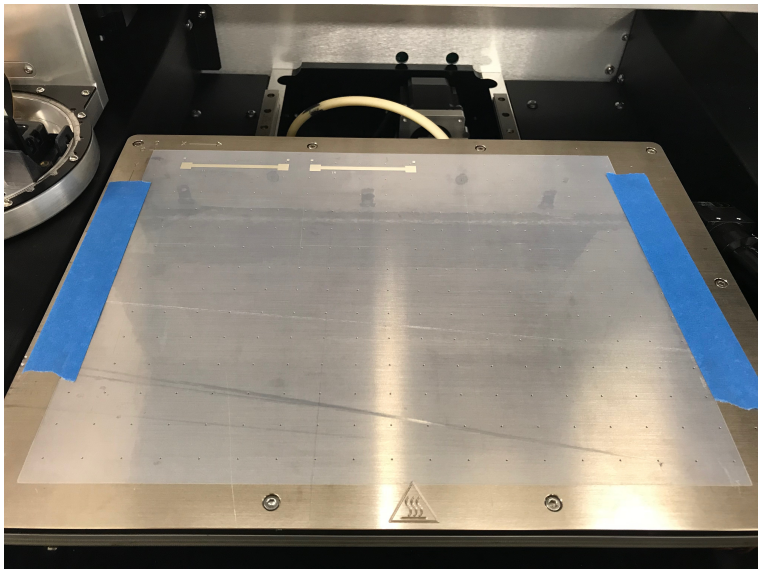

Fig. A.9. Fix The Substrate On Platen

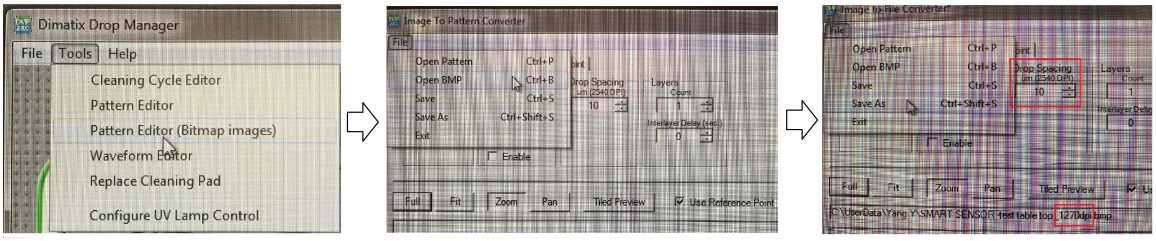

Fig. A.10. Convert The Image File

5. As shown in Fig. A. 10, generate the compatible image file using the built-in Image To Pattern Converter. Make sure to check the table 5-1 of the DMP manual for the drop size that matched with the image file resolution. Load the compatible image file. Following the instructions that shown on software GUI, adjust the sabre angle of the cartridge by rotating the inner plate (Fig. A.11). The details is described in Cartridge Mounting Angle of Chapter 5 of the DMP manual.

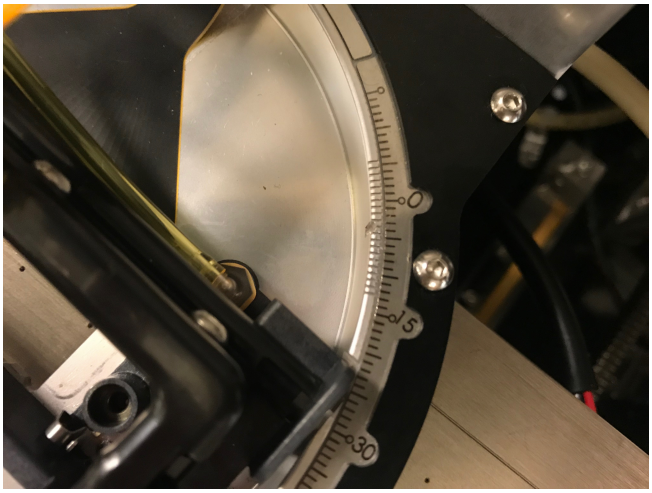

Fig. A.11. Sabre Angle Adjustment

6. Select the waveform file and the substrate thickness which are provided by the ink and substrate manufacturers on the GUI. Then, open the drop watcher (Fig. A.12.) check if the 16 printheads are working properly. (When the drop is going down with a straight tile as shown in Fig. A.12, the printhead is considered to be work well.) Turn on continuous 8 printheads for printing by checking the check box marked in the red square in Fig. A.12, while the rest of them are tuned off. If fewer than 8 printheads work well, do cleansing cycle until at least contiuous 8 printheads are ejecting ink properly.

7. Open fiducial camera (Fig. A.13.) and set the print origin. And then it is ready to print. My rule is to print one row of the electrodes (two electrodes) and then check the working condition of printheads with drop watcher.

A.3 Key Points

1. In order to preserve the nature of the ink, ink containers are glass bottles.

2. If resolution of the target printing figure is over 2540 dpi, use other software to generate the bit map file since Illustrator cannot output images with resolutions higher than 2540 dpi.

3. Before printing, make sure the ink bottle or the cartridge with ink has been put in room temperature for at least 20 minutes.

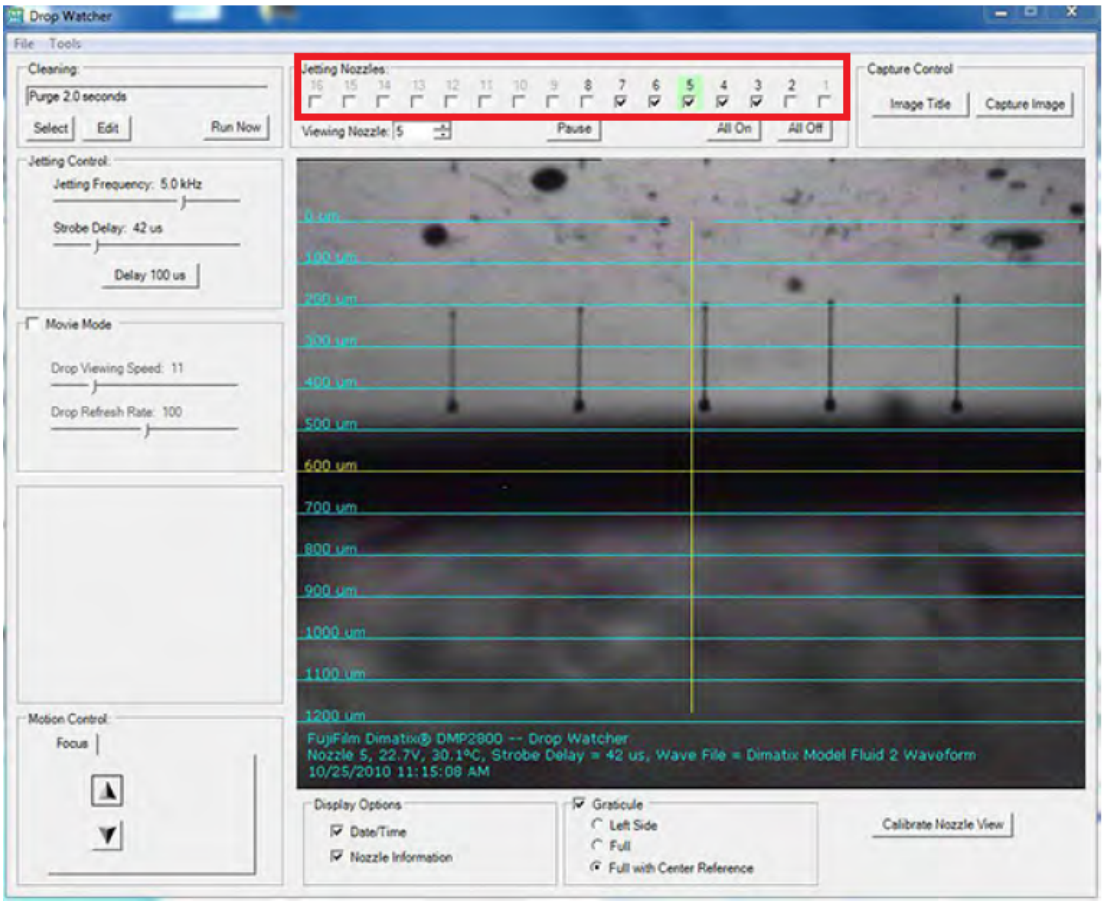

Fig. A.12. Drop Watcher

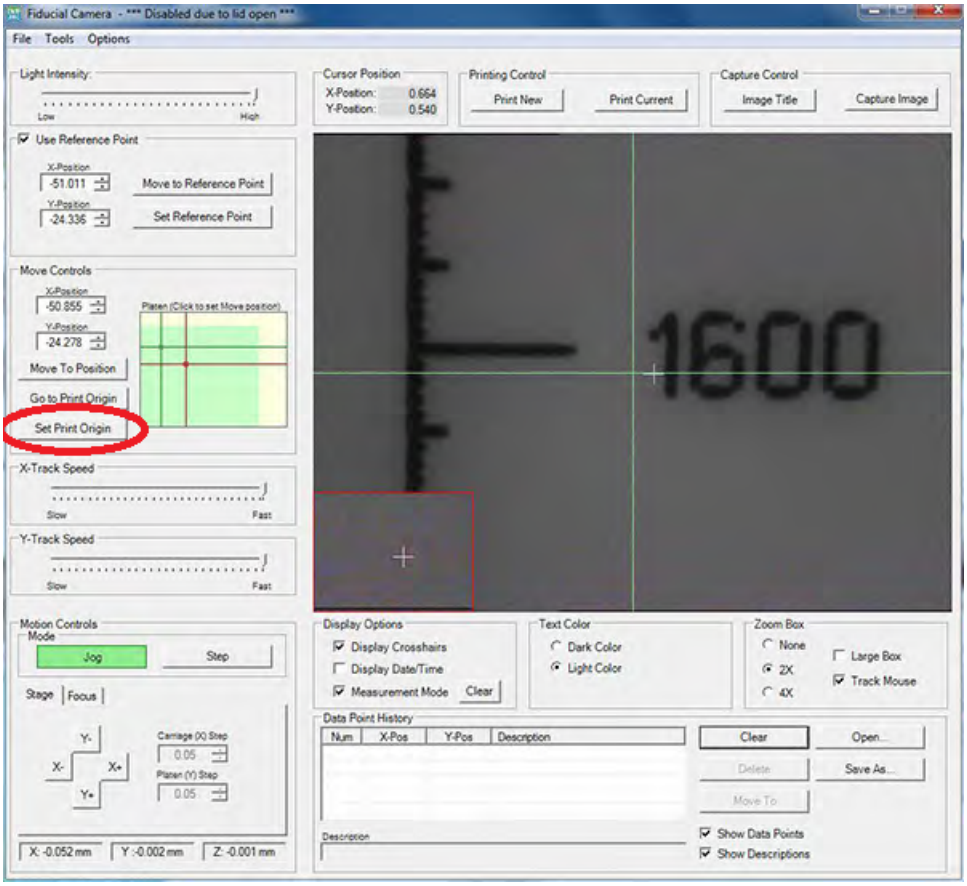

Fig. A.13. Fiducial Camera

B. JANDEL MULTI-HEIGHT PROBE OPERATING PROCEDURES

Jandel Multi-Height Probe device is shown in Fig. C.1.

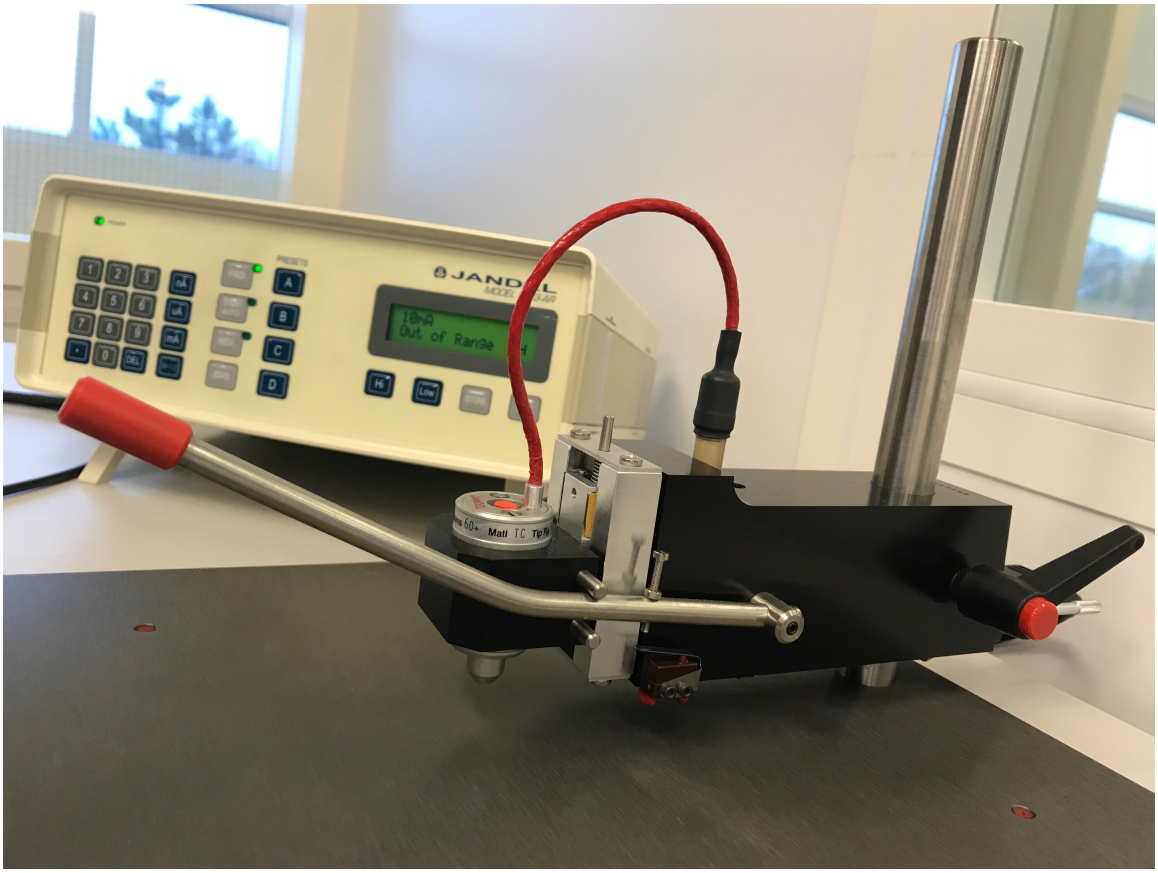

Fig. B.1. Jandel Multi-Height Probe

1. Slide off the dust-cover from the unit.
2. Turn unit on. The switch is located on the rear left hand side.
3. Carefully slide the sample to be measured under the probe using Teflon tweezers.

4. Lower the probe head carefully using the lever on the right of the head. Lower it till you hear a click. This is the micro switch that will allow measurement current to flow through the probes.

5. Enter the appropriate test current value by using the key pad or use one of the presets (A: 10 nA, B: 100 nA, C: 10 μA, D: 10 mA). The presets used here is "D".

6. Once you have desired current setting, press "FWD" to cause the current to flow through the sample. This should show a positive voltage reading. You could press REV to make the current flow in the reverse direction. In this case, the voltage will have a negative value. The sheet resistivity should have the save value of both cases.

7. Note down the values from the display. You can get the measured voltage in mV or the sheet resistance in Ω^2 by toggling the "Ω/" button.

8. On completing the measurement, raise the probe head using the lever to the top of its range of motion.

9. Gently and carefully slide out your sample with the Teflon tweezers.

10. Repeat from 4 if you need to make more measurements.

11. On completion of the measurements, turn off the unit and cover with the dust cover.

Tips:

1. The system has been set up to measure samples $500\mu m$ high.

2. Do not use with samples with a height ¿$500\mu m$.

3. Consult instructions manual with Aamer Mahnmood (amahmood@purdue.edu) for further details.

C. IMAGING PORCEDURES

The imaging procedures listed here are for imaging the area where the sheet resistance measurements are taken on Inkjet printed electrodes.

1. The camera used here is a USB 3.0 Camera (EO1312 Color USB 3.0 Camera from Edmund Optics). The lens used here is a telecentric lens with 0.5 time magnification (TECHSPEC Compact Telecentric Lens 63-741). Make sure the lens is in-line version. And the light source is a intensity adjustable light source with fiber optic wire outputs (Fiber-Lite PL900).

2. Assemble the camera and the lens. Attach the camera and lens unit on a fixed frame or stand. When attaching the unit, make sure the unit is fixed vertically versus the imaging surface.

3. Insert the light source output wire to the light socket of the lens tightly.(Fig. B.1.)

Fig. C.1. Lens

4.Put the silicon wafer on the stage or platform for imaging and put the image targeting area on top of the silicon. Make sure the bright and shine side of silicon wafer is facing up. Using weights around the image targeting area, keep the imaging area flat.

4. Open the uEye cockpit software which is provided by Edmund Optics. Under the "image" tab in the menu bar, click the "properties". Remove all the pre-processes including filters, gamma correction, and color corrections. And adjust the exposure time according to the current view of imaging.

5. Capture images with proper and fixed exposure time. Save the images in a selected directory.